Front. Mech. Eng. 2025, 20(5): 32
https://doi.org/10.1007/s11465-025-0848-0

REVIEW ARTICLE

Micro/nano functional structure manufacturing from difficult-to-cut materials by etching and its combined machining strategies: A review

Xiaoqiang YAO[a,b], Tianfeng ZHOU (✉)[a,c], Xuanzhe YANG[a], Xinbo SU[a], Qian YU[a], Weijia GUO[a], Peng LIU[a,c], Bin ZHAO[a,c], Xibin WANG[a]

[a] School of Mechanical Engineering, Beijing Institute of Technology, Beijing 100081, China
[b] School of Mechanical Engineering, Xinjiang University, Urumqi 830017, China
[c] Chongqing Innovation Center, Beijing Institute of Technology, Chongqing 401120, China
✉ Corresponding author. Email: zhoutf@bit.edu.cn (Tianfeng ZHOU)

© The Author(s) 2025. This article is published with open access at link.springer.com and journal.hep.com.cn

ABSTRACT Micro/nano functional structures (MNFSs) have attracted substantial attention because of their outstanding performance in optical, tribological, thermal, electronic, and biomedical applications. Despite the development of various mechanical and non-mechanical machining methods, achieving the high-efficiency, high-precision fabrication of MNFS from difficult-to-cut materials remains a significant technical challenge. This review begins with an introduction to typical artificial MNFSs and their stringent requirements and then provides a comprehensive survey of MNFSs, focusing on etching methods. In particular, plasma etching demonstrates notable advantages in MNFS fabrication. However, two critical challenges persist: accurately controlling topographical information during pattern transfer in plasma etching and achieving high-quality, uniform patterning masks over large areas. These issues are addressed by thoroughly analyzing and summarizing the modeling of plasma etching and the simulation of feature profiles. Various hybrid etching machining (HEM) strategies, including laser and etching combined machining, cutting and etching combined machining, molding and etching combined machining, and self-assembly and etching combined machining, are categorized and compared in detail to facilitate the manufacturing of complex MNFSs. Finally, this review summarizes current deficiencies and future challenges of HEM, laying the groundwork for further advancements in MNFS fabrication and intelligent HEM technologies.

KEYWORDS micro/nano functional structures, hybrid etching machining, difficult-to-cut material, pattern transfer, material removal mechanism

1 Introduction

All matter in the universe possesses distinct dimensions, ranging from macro to meso, micro, and nanoscale (Fig. 1). These dimensions are categorized into macrostructures, mesostructures, microstructures, and nanostructures, respectively. Inspired by the functional surfaces of biological structures, artificial micro/nano functional structures (MNFSs) have garnered significant attention [1–4]. These structures comprise repetitive geometric units spanning one or more scale ranges, such as groove arrays, lens arrays, pyramid arrays, pore arrays, and cone arrays. The unique structural features of MNFSs endow surfaces with various functionalities, including optical, tribological, thermal, electronic, and biomedical properties. As a consequence, MNFSs have attracted considerable interest from researchers. The unique structural features of MNFSs have enabled their remarkable performance in a wide range of areas, such as structural color [5], anti-reflection [6], drag reduction [7,8], wear resistance [9], anti-icing [10], antifogging [11], oil–water separation [12], liquid manipulation [13], self-cleaning [14], supercapacitors and electrode [15], sensors [16], antibacterial reaction [17], and cell adhesion [18].

With the swift advancement of cutting-edge optical

Received November 1, 2024; accepted December 19, 2024; online September 19, 2025

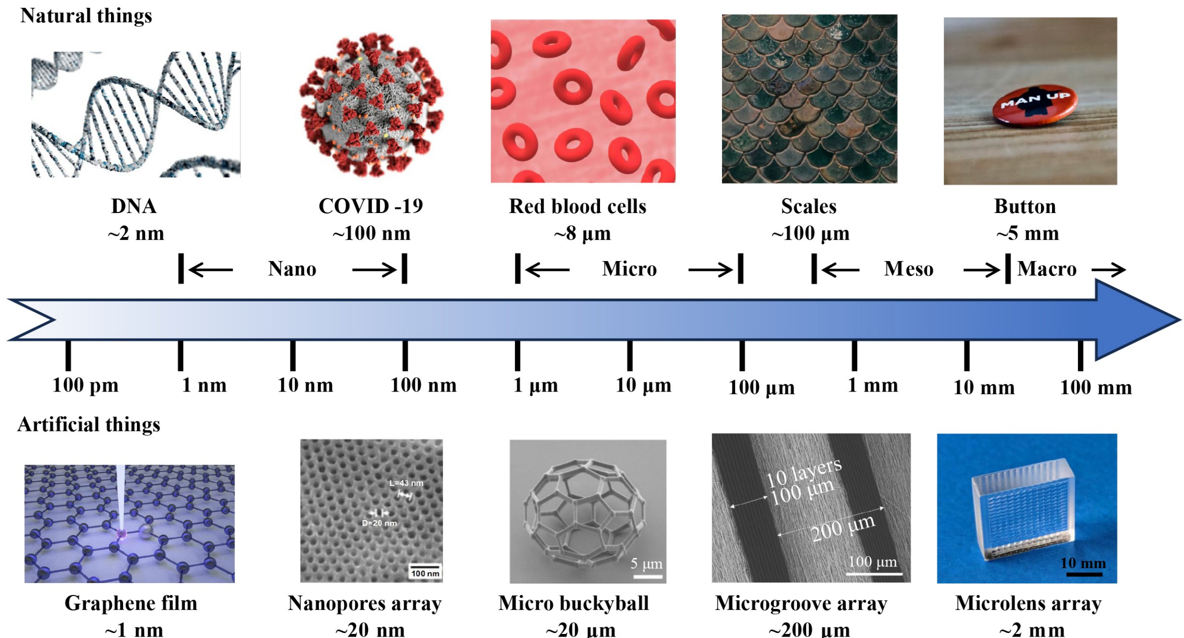

Fig. 1 Natural and artificial entities at different scales [1–4]. Reproduced from [1] with permission from Elsevier. Reproduced from [2] with permission from John Wiley & Sons. Reproduced from [3] with permission from Optica Publishing Group. Reproduced from [4] under CC BY 4.0 license.

and electronic technologies in industries such as semiconductors, photonics, and aerospace, MNFS fabrication on difficult-to-cut materials (DCMs), such as superalloys, glass, ceramics, and crystals, holds great importance. Such components require ultraprecision machining with minimal damage to satisfy the stringent application demands in these domains. DCMs are characterized by high strength, chemical inertness, and excellent wear resistance. However, these properties also render them notoriously challenging to machine, often complicating efforts to maintain surface integrity. Therefore, MNFS fabrication on DCMs remains a substantial and unresolved challenge for modern manufacturing industries.

Mechanical and non-mechanical approaches have advanced swiftly to address the challenges of MNFS fabrication on DCMs. Mechanical machining techniques play a crucial role in MNFS fabrication. Among these methods, ultra-precision cutting and grinding are particularly prevalent. These methods utilize diamond tools or abrasives to achieve material removal at micro/nanoscale levels, enabling the precise fabrication of desired structures [19,20]. However, this technology is limited by material machinability and processing efficiency. By contrast, laser technology offers superior material adaptability. Laser-induced periodic surface structures demonstrate significant efficiency in MNFS fabrication. Nevertheless, achieving an optimal balance between high efficiency and precision remains a challenge [21]. Micro-electrical discharge machining and micro-electrochemical machining have also been explored for producing MNFS with high aspect ratios and complex geometries [22]. Known for its ability to achieve atomic-scale material removal, etching provides high efficiency and precision in manufacturing. Compared with wet etching, dry etching offers enhanced flexibility and controllability. According to their surface reaction mechanisms, dry etching methods are categorized into ion beam etching (IBE), reactive ion etching (RIE), and plasma chemical etching. As the standard process for integrated circuit manufacturing, etching is commonly used in conjunction with lithography to fabricate simple microstructure arrays [23]. The manufacturing of complex MNFSs that require cross-scale, large-area, high-efficiency, and high-precision techniques still presents significant challenges. Various hybrid etching machining (HEM) strategies, including laser and etching combined machining (LEM), cutting and etching combined machining (CEM), molding and etching combined machining (MEM), and self-assembly and etching combined machining (SAEM), have been developed to address these issues.

MNFS fabrication using HEM strategies has been the focus of numerous published studies, as depicted in Fig. 2. However, systematic reviews on this topic are scarce. The present review aims to offer a comprehensive summary of recent advancements in the fabrication, theory, and application of MNFSs prepared via HEM. We begin with a brief discussion

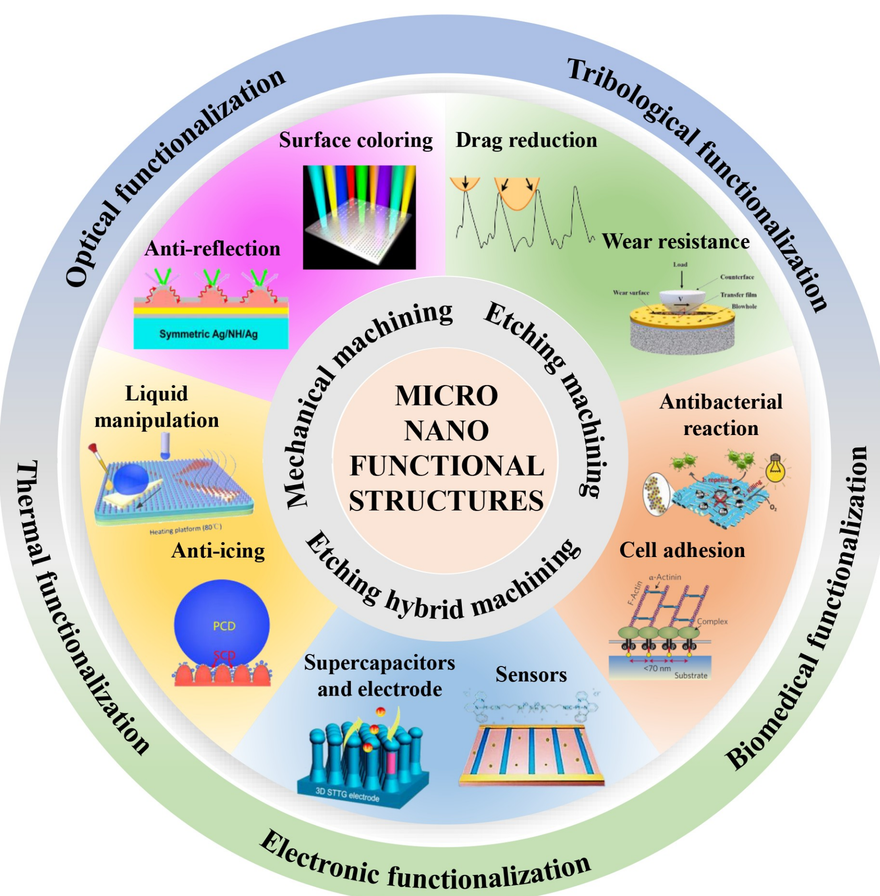

Fig. 2 Overview of MNFSs and their fabrication strategies and application [5,6,8–10,13,15–18]. Reproduced from [5] with permission from Springer Nature. Reproduced from [6] under CC BY 4.0 license. Reproduced from [8] under CC BY 4.0 license. Reproduced from [9] with permission from Elsevier. Reproduced from [10] with permission from American Chemical Society. Liquid manipulation [13], reproduced with permission from RSC Publishing. Reproduced from [15] with permission from American Chemical Society. Reproduced from [16] with permission from John Wiley & Sons. Reproduced from [17] with permission from American Chemical Society. Reproduced from [18] with permission from Springer Nature.

on the applications of MNFS, followed by an examination of their corresponding structural features. Next, we systematically summarize and evaluate HEM strategies. We also provide a detailed introduction to the modeling and simulation of pattern transfer using etching, addressing the key issues in precision control encountered during this process. Finally, we discuss the difficulties and challenges faced in MNFS fabrication using HEM strategies. By outlining these advancements and presenting our perspectives, we aim to offer researchers a comprehensive and nuanced understanding and pave the way for the practical application of MNFSs.

2 Typical MNFSs and their applications

To thrive in complex environmental conditions, plants and animals have developed a diverse range of structural features. Inspired by these biological microstructures, various MNFSs have been developed, making them a noteworthy research focus in the field of surface interfaces. This section offers an overview of representative artificial MNFSs, including prism arrays, pillar/cone arrays, pole/dimple arrays, lens arrays, pore/dimple arrays, and hierarchical arrays. A brief introduction to their manufacturing methods and applications is also provided (Fig. 3).

2.1 Prism arrays

Prism arrays are a prominent category of MNFSs, with notable examples including groove arrays and pyramid arrays. These structures are further classified based on their cross-sectional shapes as V-groove, rectangular groove, and circular groove arrays. Inspired by the surface texture of rice leaves, the varying frictional forces between parallel and

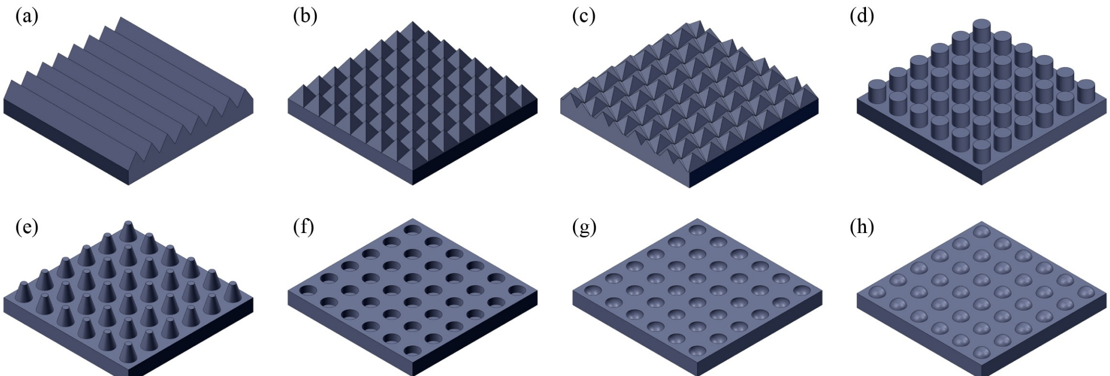

Fig. 3 Typical artificial MNFSs: (a) groove array, (b) pyramid array, (c) prism array, (d) pillar array, (e) cone array, (f) pore array, (g) dimple array, and (h) lens array.

perpendicular grooves cause droplets to preferentially flow along the direction of the parallel grooves [24]. Moreover, groove arrays within specific size ranges can be employed to achieve fiber alignment [25], induce structural colors [26], and enhance luminescence efficiency [27]. Recognized for their excellent anti-reflective properties, pyramid arrays are widely used in the photovoltaic industry [28].

Various methods exist for fabricating prism arrays, with ultra-precision cutting being one of the most commonly employed. Our research team comparatively evaluated the machining efficiency and precision of planning and fly-cutting fabrication methods for V-groove and pyramid arrays [29]. Although femtosecond laser techniques can achieve high efficiency, they are constrained by the processing quality and flexibility [30,31]. LEM has been utilized for fabricating groove arrays to improve the processing quality [32,33]. Furthermore, the anisotropic properties of single-crystal materials have been leveraged in wet etching. This approach has enabled the production of complex structures, including pyramids [28] and prisms [34].

2.2 Pillar/cone arrays

Pillar and cone arrays are frequently observed in nature, particularly on the footpads found in various large species (such as geckos, tree frogs, and insects) and displaying remarkable adhesive properties across diverse environments [35]. This observation has inspired the development of numerous artificial pillar and cone arrays for adhesion enhancement and hydrophilic regulation. Current research has further expanded the application of these arrays to areas such as optical field modulation [36] and temperature sensors [37].

Owing to its compatibility with these structures, lithography is extensively utilized in the fabrication of pillar arrays [36,38]. However, traditional lithography encounters resolution limits that constrain its effectiveness in processing large-area nanopillar arrays. Nanosphere lithography, which relies on the self-assembly of nanospheres, has gained prominence for the production of nanopillars and nanocones without the above limitation [39]. Techniques utilizing anodic aluminum oxide (AAO) are also employed to efficiently fabricate large-area nanopillar arrays [40].

2.3 Pole/dimple arrays

Pole and dimple arrays are another prevalent type of MNFSs found in nature. With advances in technology, these arrays have been extensively applied in fields such as biosensing, sensors, light-emitting devices, and renewable energy [41–44]. For example, nanopore sequencing enables the complete genomic sequencing of the human body [45] and facilitates disease prediction, diagnosis, and drug screening [44]. Furthermore, nanopore and dimple arrays have been extensively used in electrode materials [46] and cell culture [47].

At the microscale, lithography is commonly employed to fabricate pore arrays. For nanoscale fabrication, various HEM strategies are utilized to process nano pit and pore arrays [48]. A widely used technique for creating nanopore arrays is anodic oxidation, in which an electric current is applied to a metal or alloy to produce an oxide layer through electrolysis. Vertically aligned nanopore arrays can be obtained by placing aluminum in an appropriate electrolyte [49]. Laser technology and laser-assisted techniques have also been employed in the fabrication of nanopore arrays to enhance material compatibility [50,51].

2.4 Lens arrays

Lens arrays are a fundamental component of MNFSs,

playing a pivotal role in advancing optical technologies. These arrays contribute to the miniaturization of photonic systems and enhance the functionality of imaging and sensing devices [52]. With the increasing demand for integrated, compact, and intelligent devices, the manufacturing of microlens arrays (MLAs) with large formats, high efficiency, and small dimensions has received growing interest.

At present, ultra-precision machining is the predominant method for fabricating MLAs [53,54]. However, challenges remain in the processing of DCMs such as SiC, Si, and sapphire. Although laser processing provides efficient removal for these materials, it often falls short of delivering the precision required for high-quality fabrication. LEM offers a viable solution to this problem [55–57]. Various lithography techniques, including ultraviolet (UV) lithography, grayscale lithography, and thermal reflow, are also effective for fabricating MLAs on hard and brittle materials [58–61].

2.5 Hierarchical arrays

With the growing diversification and integration of demands for MNFSs, hierarchical structures with multiple functions have been designed and fabricated by arranging micro- and nanoscale elements along periodic pathways in space. These structures offer a range of functionalities, including anti-icing [10], antireflection, enhanced transparency [6], and superhydrophobicity [62]. Furthermore, they facilitate the integration of multiple functions, such as geometric and diffraction optics [63].

Researchers investigated fabrication techniques for hierarchical arrays, with ultra-precision machining being extensively utilized. For instance, Zhu et al. [64] fabricated a hierarchical micro-nanostructure by integrating slow tool servo techniques with fly cutting. Our research team utilized ultrasonic vibration-assisted fly cutting to manufacture multilevel groove array structures [65]. In contrast to ultra-precision machining, laser technology offers enhanced efficiency. Hu et al. [66] effectively showcased the production of hierarchical array structures on SiC wafers through laser technology. HEM has also been widely applied in the production of hierarchical structures [67,68].

In summary, numerous artificial functional structures inspired by natural designs have been developed, each demonstrating significant potential for various applications. This review presents a comparative and classificatory analysis of the prevalent forms, fabrication methods, and application domains of MNFSs as detailed in Table 1. These insights aim to guide future investigations and provide a solid foundation for the application of MNFSs across diverse fields, including aerospace, marine technology, energy, environmental science, and biomedicine. Future investigations will focus on elucidating the relationship between these structures and their functionalities to elucidate the mechanisms underlying their performance. A broad range of MNFSs, particularly hierarchical MNFSs, is expected to attract increasing attention from researchers.

3 Etching techniques for MNFS fabrication

Etching, a critical step in integrated circuit fabrication, is generally divided into two primary types: dry and wet etching. Dry etching methods are further categorized based on their surface reaction mechanisms into plasma chemical etching, RIE, and IBE. The following section provides a detailed discussion of the material removal mechanisms and specific surface reaction processes. In dry etching, the etchant is introduced in the vapor phase for enhanced precision and control. By contrast, wet etching involves the removal of material from a surface using a chemical solution. A liquid etchant is used to selectively dissolve the target material through a chemical reaction, making it a simple process that can be performed using basic laboratory equipment.

Dry and wet etching techniques facilitate the fabrication of 3D structures with diverse topographical features, which are influenced by the choice of masking materials and specific etching parameters. This section offers a comprehensive review of essential etching methods and masking approaches, including UV lithography, grayscale lithography, and thermal reflow-assisted etching, which are employed to achieve precise and controlled surface morphologies in DCM microfabrication.

3.1 UV lithography-assisted etching

UV lithography is a widely used 2D mask patterning technique. When combined with etching, it enables the fabrication of various types of MNFSs, such as cavities, MLAs, and cylindrical arrays [77,89,95] (Fig. 4(a)). This hybrid fabrication approach is referred to as UV lithography-assisted etching.

Wet etching facilitates the isotropic etching of amorphous and polycrystalline materials. When combined with traditional UV lithography techniques, it facilitates MLA fabrication. For materials such as polycrystalline Si and glass, the wet etching process is isotropic. Zhang et al. [58] utilized wet etching to create spherical arrays and sharp ribs on the surface of a quartz substrate, as shown in Fig. 4(c). For single-crystal materials such as silicon and gallium

Table 1 Representative artificial MNFSs and their applications

Classification	Applications	Fabrication methods	References
Groove array	■ Grating ■ Drag reduction ■ Optical fiber positioning ■ Antireflective performance	Laser processing	[30,31,69,70]
		Ultra-precision machining	[26,29,71,72]
		LEM	[32,33,73]
		MEM	[74,75]
Pyramid array	■ Hydrophilic regulation ■ Anti-wear ■ Antireflective performance	Ultra-precision machining	[29]
		Lithography and wet etching	[28,76,77]
Pillar/core array	■ Adhesion enhancement ■ Optical field manipulation ■ Sensor ■ Hydrophilic regulation	Lithography and dry etching	[78,79]
		SAEM	[80–82]
Lens array	■ Optical homogenization ■ Optical imaging ■ Wavefront sensing ■ Optical interconnections ■ Liquid crystal displays	Ultra-precision machining	[53,54,83]
		MEM	[84]
		CEM	[85,86]
		LEM	[55–57,87,88]
		Lithography and wet/dry etching	[89,90]
		SAEM	[91,92]
Pore/dimple array	■ Gene sequencing ■ Cell culture ■ Electrode material ■ Sensor	Lithography and dry etching	[93]
		Anodic oxidation	[94]
		Laser processing	[50]
Hierarchical array	■ Antireflective performance ■ Hydrophilic regulation ■ Droplet manipulation ■ Self-cleaning	Ultra-precision machining	[64,65]
		SAEM	[67,68]
		Laser processing	[66]

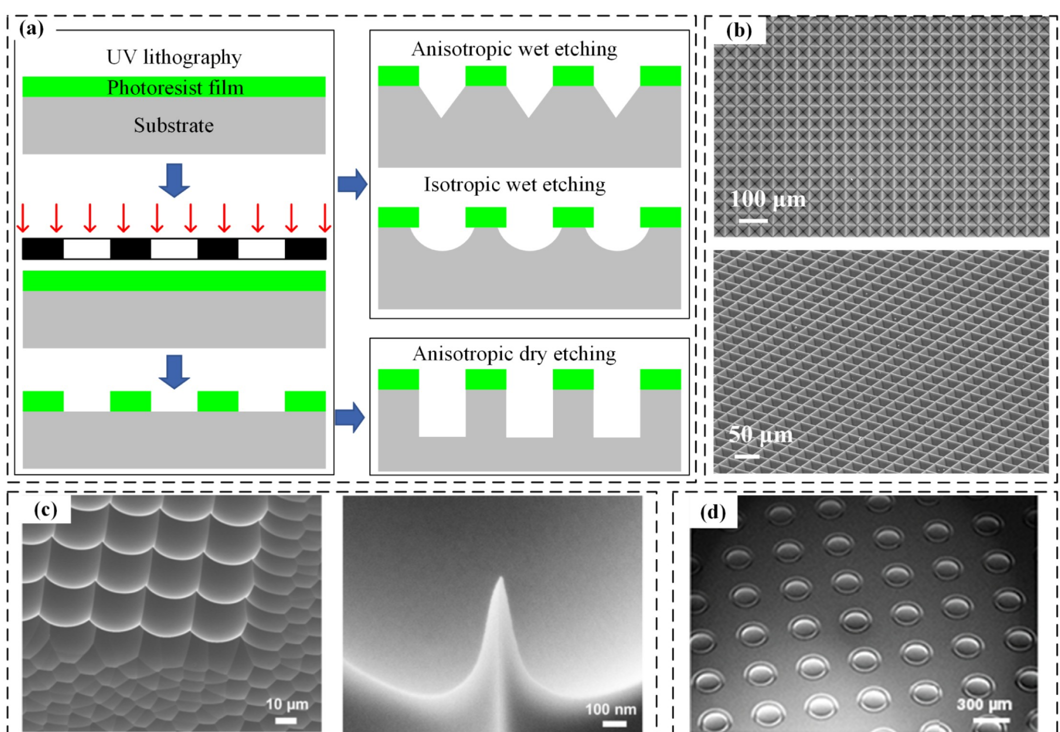

Fig. 4 MNFS fabricated by UV lithography-assisted etching: (a) Schematic of UV lithography-assisted etching. (b) Si micropyramid array fabricated by anisotropic wet etching [77]. Reproduced with permission from Elsevier. (c) MLA manufacturing by isotropic wet etching [89]. Reproduced with permission from IOP Publishing. (d) Cylindrical array using dry etching [95]. Reproduced with permission from IOP Publishing.

nitride, the etching rates vary with crystal orientation because of differences in atomic bonding and arrangement. Anisotropic wet etching methods can be employed to produce various pyramid array structures [28,77] (Fig. 4(b)) and nanotip pyramids [96] on Si crystals and hexagonal [34] and cavities [97] on GaN and quartz crystals.

Dry etching techniques exhibit high anisotropy, allowing for precise pattern transfer. When paired with UV lithography, the enhanced material removal anisotropy in dry etching has successfully enabled the fabrication of 2D and high-aspect-ratio structural arrays, including groove arrays [98], cylindrical arrays [95] (Fig. 4(d)), and pillar/cone arrays [99] across various materials. Although UV lithography can generate a wide variety of high-quality MNFSs, the fabrication of complex MNFSs using 2D masks remains challenging.

3.2 Grayscale lithography-assisted etching

Grayscale lithography represents a significant advancement over conventional lithography. It utilizes a specific mask or direct-writing technique to achieve varying exposure doses across different locations on the same photoresist film. This differential exposure leads to the development of photoresist structures with 3D profiles [100]. The mask used in this process is known as a grayscale mask. Grayscale exposure technology encompasses electron beam lithography [101], laser direct writing [102], and conventional lithography [61,103] with grayscale masks. As this technology continues to evolve, its precision in 3D patterning also improves.

Figure 5 presents the MNFSs fabricated via grayscale lithography-assisted etching [104,105]. As depicted in Fig. 5(a), Bekker et al. [104] developed an

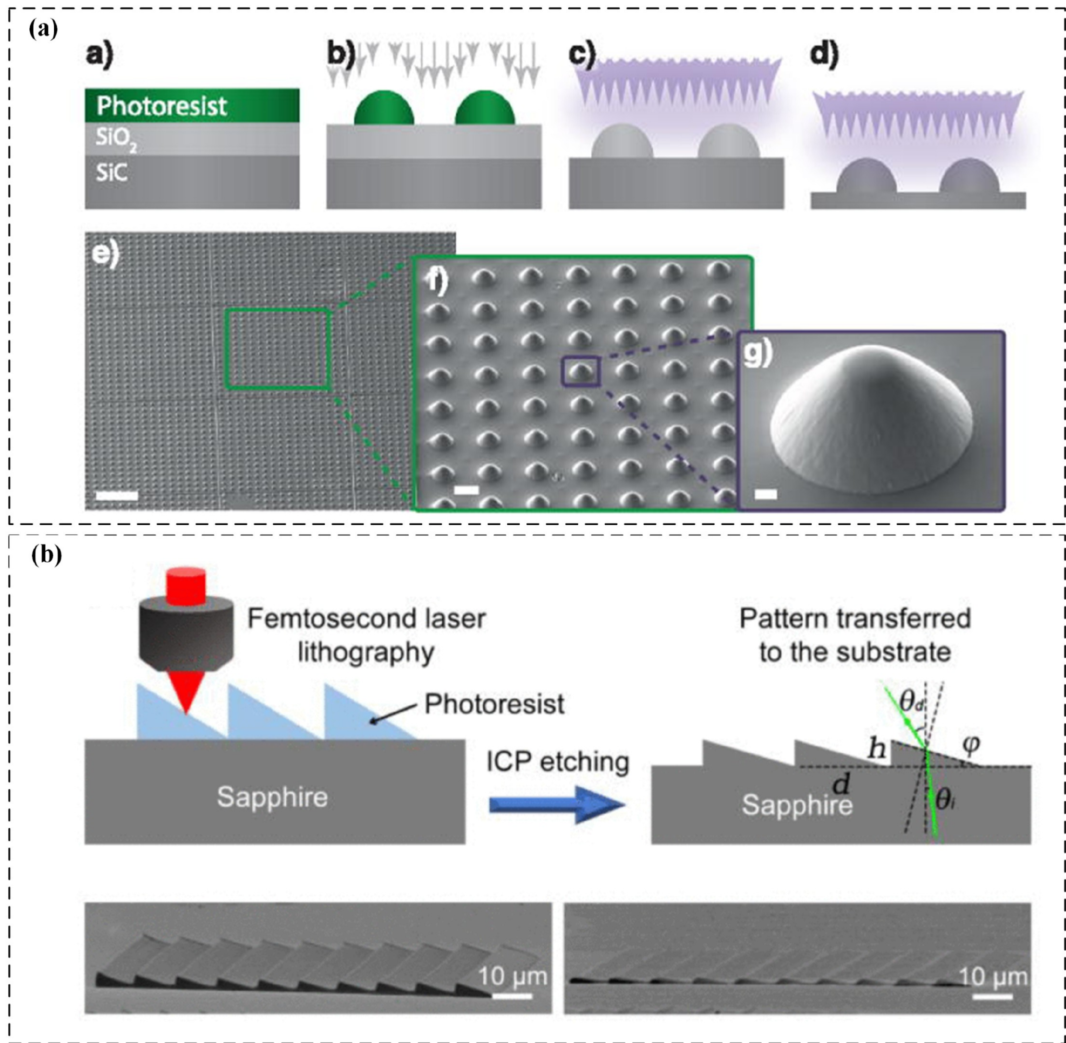

Fig. 5 MNFSs fabricated by grayscale lithography: (a) Fabrication protocol for solid immersion lenses in SiC by grayscale hard-mask lithography [104]. Reproduced with permission from AIP Publishing. (b) Fabrication of sapphire blazed gratings by etching-assisted femtosecond laser lithography [105]. Reproduced with permission from IEEE. Scale bars in subfigure (a) represent 100, 10, and 2 μm, respectively.

innovative method that combines grayscale lithography with hard-mask techniques to fabricate a solid immersion lens in SiC. Although this method maintains the scalability and effectiveness characteristic of lithography-based approaches, achieving precise control over the fabricated structures continues to be a significant challenge. Figure 5(b) illustrates the fabrication of sapphire blazed gratings by etching-assisted femtosecond laser lithography [105]. Although laser direct writing offers high precision, its low processing efficiency significantly limits its further applications. In addition, this technique has increasingly been employed for fabricating Fresnel lenses [106] and various complex freeform optical structures [102,107]. However, the complex pattern transfer during plasma etching complicates the achievement of precise control over the surface profile.

3.3 Thermal reflow-assisted etching

Thermal reflow involves heating photoresist beyond its glass transition temperature, resulting in softening and deformation due to surface tension [108]. This transition is achieved by heating the initial structure to a state where the material can flow. Once cured (cooled), the material retains its new shape, which is influenced by surface tension. This phenomenon converts the initially energy-unfavorable structure into a smooth configuration with minimal surface energy. This technique yields low surface roughness, which is advantageous for the industrial production of MLAs.

The combination of thermal reflow and etching (Fig. 6(a)) has proven effective in fabricating MLAs on various materials. Lee et al. [59] successfully fabricated microlenses on SiC using this method, achieving shape control through adjustments in etching selectivity. This technology has also been applied to other materials, including Si [60,109], glass [60], and diamond [110,111] for MLA fabrication. However, this technique is limited to the production of spherical MLAs, and the mechanism of shape control is complex and requires further research.

Whether through lithography for 2D mask or 3D mask structures, MNFSs can be fabricated on DCMs via pattern transfer. In the case of 2D masks, MNFS is primarily created through anisotropic etching induced by the interactions between the etching solution or plasma and the target material. Meanwhile, 3D masks facilitate the fabrication of complex MNFSs by establishing a direct correlation between the shapes of the mask and substrate under specific process parameters. Therefore, the accurate kinetic modeling of the etching process and the efficient, large-area production of mask-relief structures are essential to the success of etching-based hybrid processing. These aspects will be discussed in detail in the subsequent sections.

4 Modeling of plasma etching for shape control

The core of plasma etching for MNFS fabrication lies in the development of a mathematical model that maps the relationship between the film and substrate structures. This model facilitates the understanding and simulation of the transfer mechanisms involved in patterning complex, 3D shapes. This chapter focuses specifically on dry etching. We illustrate the modeling workflow for shape evolution in Fig. 7(a). The entire modeling process is highly complex. First, the reactor model establishes the relationships of process parameters, including source power, bias power, gas flow, and chamber pressure, with various particle densities and electron temperature. By employing a sheath model, we can determine the ion energy and angular distributions (IEADs) incident on the substrate. Subsequently, the plasma-material surface

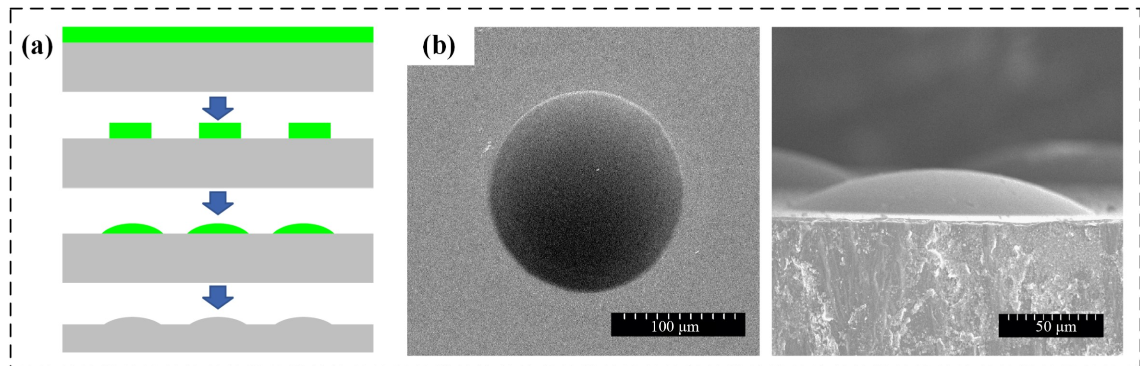

Fig. 6 MNFS fabricated by thermal reflow-assisted etching. (a) Schematic of thermal reflow-assisted etching. (b) Fabrication of MLAs on SiC [59]. Reproduced with permission from Elsevier.

reaction models based on particle transport modeling are categorized. Finally, the feature-scale simulation of pattern transfer through plasma etching is comprehensively analyzed and summarized.

4.1 Particle transport modeling

To further develop the feature-scale model, researchers extensively studied the transport models for ion and neutral fluxes within microscopic structural features [112–114]. As illustrated in Fig. 7(b), the 2D model indicates that the ions and neutral fluxes from the plasma strike the substrate and subsequently interact with the surface of the etched material.

4.1.1 Incident ion flux

In the ion transport from the sheath edge to the substrate surface, the influence of ion scattering within the sheath can be neglected in low-density, high-voltage plasma etching. Hence, the direction in which ions strike the substrate is mainly governed by the ion temperature or their random movement within the plasma. Ions at the edge of the sheath exhibit an angular velocity distribution, and the angular distribution of the ion flux incident onto the surface is described by the following expression [115]:

$$\mathrm{d}\Gamma_i = \Gamma_i^0 G_i(\theta)\cos\theta\,\mathrm{d}\theta, \tag{1}$$

where Γ_i^0 represents the ion flux at the sheath edge directed toward the substrate. The incident angular distribution of ion fluxes onto the macroscopic substrate surface, denoted as $G(\theta)\cos\theta$, is determined by the ratio R between the energy of ions accelerated across the sheath and the ion temperature. The value of R can be modified by regulating the process parameters such as electrode bias, RF power, and chamber pressure. The number of ions entering the microstructures decreases because of the shadowing effect created by the mask shape. The opening window is determined by two boundary angles, θ_1 and θ_2, which constrain the ions' straight-line trajectory to reach a specific point. As shown in Fig. 7(b), the incident ion flux at point P is expressed as

$$\Gamma_i^0(P) = \int_{\theta_1}^{\theta_2} G(\theta)\cos(\theta-\psi)\mathrm{d}\theta, \tag{2}$$

where ψ denotes the angle of the surface slope. When the shadowing effect is absent, we assume that $G_i(\theta)\cos\theta$ follows a Gaussian distribution so that

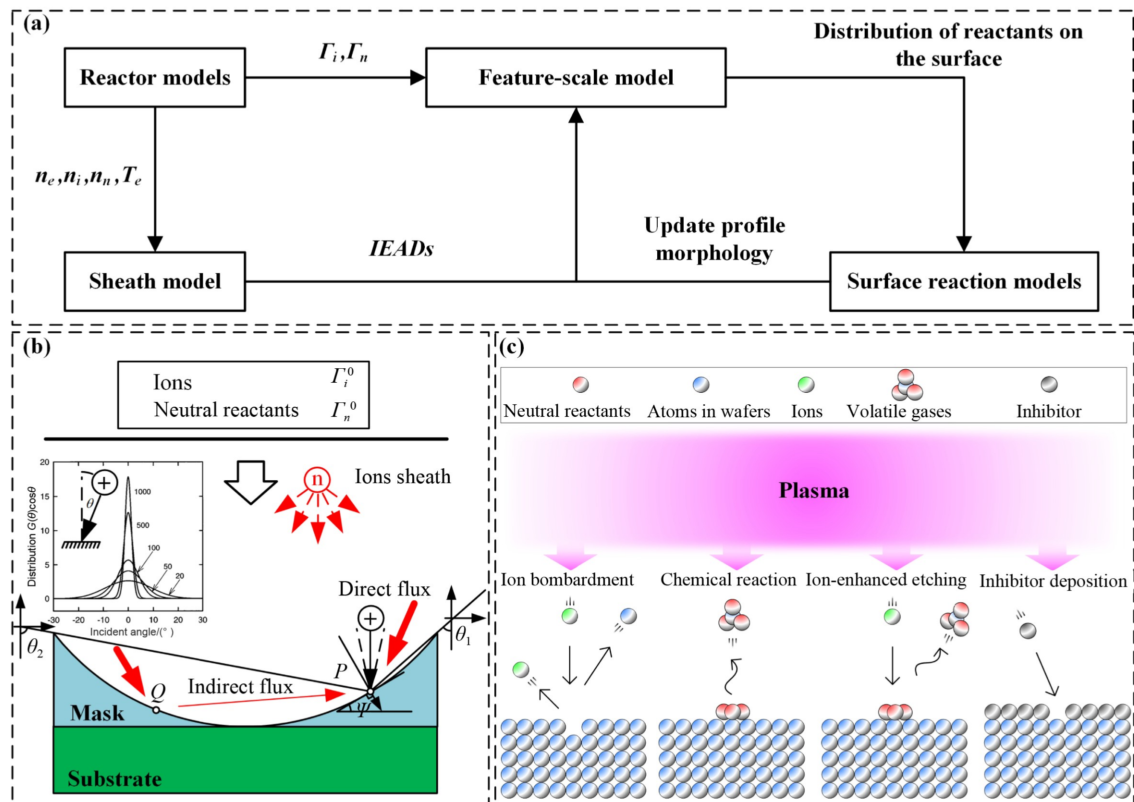

Fig. 7 Feature-scale simulation of pattern transfer through plasma etching. (a) Flow chart of profile evolution simulation. (b) Particle transportation model. (c) Surface reaction of plasma etching.

$\int_{-\pi/2}^{\pi/2} G_i(\theta)\cos\theta d\theta = 1$. Given that R is chosen to be between 300 and 500, resulting in a high concentration degree, the ion flux along the etching direction at any point P can be defined using the formula $\Gamma_i(P) = \Gamma_i^0$.

4.1.2 Neutral reactant flux

As illustrated in Fig. 7(b), neutral reactants exhibit isotropic angular distribution as they diffuse into the grooves. Upon reaching point Q on the surface, these species may either be adsorbed or reflected, depending on their adhesion probability $S_n(Q)$. We assume that the reflected angle complies with the cosine law; therefore, the reflected flux is proportional to $\cos\phi$, where ϕ denotes the angle measured from the surface normal at the point of emission. The present model indicates that adhesion probability is influenced by surface coverage, decreasing linearly with increasing coverage until it reaches zero at saturation [116]. $S_n(Q) = S_{n0}\left[1 - S_n(Q)\right]$. The surface coverage in etching is represented by

$$S_n(Q) = \frac{S_{n0}\Gamma_n(Q)}{S_{n0}\Gamma_n(Q) + S_t\Gamma_i(Q)}, \tag{3}$$

where S_{n0} denotes the sticking coefficient of neutral species on an uncovered surface, $\Gamma_n(Q)$ represents the incident neutral flux at point Q, and S_t is the total removal number of neutral during the per ion incidence. Therefore, the incident neutral flux at point P (Fig. 7(b)) is given by the following expression:

$$\Gamma_n(P) = \frac{\Gamma_n^0}{2}\int_{\theta_1}^{\theta_2}\cos(\theta-\psi)d\theta + \int\frac{\left[1 - S_n(Q)\right]\Gamma_n(Q)\cos\varphi_P\cos\varphi_Q}{2r}dl. \tag{4}$$

4.2 Surface reaction modeling

All chemical etching processes generally involve three essential steps [117]: 1) attachment of etching species on the surface, 2) generation of reaction by-products, and 3) removal of these products from the surface. During plasma discharge, diverse species are generated [118], such as charged particles (ions and electrons), photons, and neutral particles. Plasma etching of materials involves a complex interplay between chemical reactions and physical sputtering. The extent of physical and chemical reactions is primarily influenced by the process parameters. Therefore, plasma etching methods can be divided into four specific types, as shown in Fig. 7(c): physical sputtering, thermally induced plasma etching, ion-enhanced plasma etching, and inhibitor-controlled plasma etching. The total etch rate results from the combined effects of these specific types outlined above:

$$ER = \Gamma_i\varphi_S + \Gamma_n(1-\alpha-\beta)\varphi_N + \Gamma_n\alpha\varphi_N^* + \Gamma_n\beta\varphi_N^{**}, \tag{5}$$

where φ_N is the chemical etching efficiency, and φ_N^* and φ_N^{**} represent the chemical etching efficiencies on two distinct surface fractions: α, which has undergone ion bombardment, and β, which is covered by an etch inhibitor.

4.3 Feature-scale profile modeling

The evolution of interfaces between two phases in fluid dynamics has been extensively studied and applied to investigate etching interfaces. Shaqfeh and Jurgensen [119] were among the first to utilize the fluid dynamics theory to simulate the pattern transfer in RIE. If $F(\boldsymbol{x},t) = 0$ defines the initial position of the interface, then the interface position after a time increment $t+\delta t$ can be expressed as

$$F(\boldsymbol{x} + \boldsymbol{n}(\boldsymbol{v}\cdot\boldsymbol{n})\delta t, t+\delta t) = 0, \tag{6}$$

where $\boldsymbol{v}$ denotes the velocity of the interface movement, and $\boldsymbol{n}$ denotes its direction vector. For the above equation, $\boldsymbol{n} \equiv \nabla\boldsymbol{F}/|\nabla\boldsymbol{F}|$, which implies that the surface evolution equation is given by

$$\boldsymbol{v}\cdot\boldsymbol{n} = -\frac{1}{\nabla\boldsymbol{F}}\frac{\partial\boldsymbol{F}}{\partial t}. \tag{7}$$

Various methods, including string, level-set, shock-tracking, and cell removal, have been employed to predict the evolution of etching interfaces for materials such as Si, Si_3N_4, SiO_2, and SiC in 2D and 3D spaces over the scale of 100 nm to solve the partial differential equations and simulate the surface evolution during etching. The string algorithm was initially utilized to simulate the 2D morphology of planar-type MOSFETs and trench structures [120–122]. We experimentally determined and fitted the angular dependence of the mask and the substrate to model the pattern transfer in microgroove inductively coupled plasma (ICP) etching [74]. Hamaguchi et al. [123] introduced a shock-tracking algorithm to overcome the instability of the string algorithm when modeling profiles with localized variations, such as sidewall etching, microgrooves, and mask erosion. This approach introduces additional entropy conditions to ensure the stable progression of the etching front within the string algorithm. The level-set method serves as a refined variant of shock-tracking, significantly enhancing the accuracy and stability of etching evolution. Its stable compatibility with simulations of 3D structures further contributes to its utility in advanced

applications. Ichikawa et al. [124] utilized the 3D level-set method, which accounts for the transport of ions and neutrals, to simulate the RIE of high-aspect-ratio structures and revealed the mechanism of etching residues in pattern corners. Cell removal methods are widely employed in feature-scale modeling because of their flexibility and compatibility with Monte Carlo gas transport. Guo and Sawin [125] developed a kinetics model for SiO_2 etching in C_4F_8/Ar gas plasma and then incorporated it into a 3D cell removal profile simulator based on Monte Carlo.

In summary, etching techniques can be utilized to fabricate a diverse array of MNFSs on DCMs. Compared with wet etching, dry etching provides advantages such as higher precision and improved control, making it the preferred method for processing MNFSs. However, due to limitations in material properties, UV lithography and thermal reflow techniques are generally restricted to processing specific MNFSs such as lens arrays and prism arrays. Although grayscale lithography can produce complex 3D structures, its processing quality and efficiency still require significant improvement. The modeling and simulation of plasma etching have advanced from simple 2D trench structures to complex 3D structures composed of heterogeneous materials. Hence, additional mask patterning techniques are urgently needed to facilitate the efficient, high-precision, and large-scale fabrication of intricate MNFSs.

5 HEM strategies for MNFS fabrication

HEM, a cutting-edge technique, is widely utilized for MNFS fabrication. This approach comprises two main components: surface patterning and pattern transfer through etching. Specific mapping relationships are employed to convert patterns from the initial surface into structures with predefined designs. These mapping relationships encompass proportional scaling in multiple directions and complex transformations between different shapes. This section presents a systematic review of HEM strategies, including LEM, CEM, MEM, and SAEM.

5.1 Laser and etching combined method

5.1.1 Laser and wet etching combined method

LEM represents a prominent hybrid technique for fabricating MNFSs. This approach integrates femtosecond laser surface modification with chemical wet etching as illustrated in Fig. 8(a). Initially introduced by Marcinkevičius et al. [126], this technique was employed to create microchannels on Si substrates. Since its inception, considerable efforts have focused on refining its process parameters and expanding its applications. Chen et al. [56] successfully utilized this method to fabricate MLAs on hard and brittle materials such as Si (Figs. 8(b) and 8(c)), SiO_2, and BK7 glass [127]. Zhou et al. [57] demonstrated its application in fabricating MLAs on chalcogenide glass. This method leverages the tendency of femtosecond laser-modified regions to evolve into spherical shapes during prolonged isotropic wet etching.

In addition to MLA fabrication, this technique has been further developed for creating microgrooves and curved compound eye array structures [128]. Li et al. [32] proposed the laser-guided anisotropic etching (LGAE) technique illustrated in Fig. 8(d). The process begins with an ultrafast Bessel beam generating high aspect-ratio, line-shaped modifications, which are then etched directionally along the modified paths to produce V-shaped profiles with controlled angles. Finally, LGAE is used to fabricate flexible microgrooves and micropyramid array structures on glass, as shown in Fig. 8(e). These innovations have significantly expanded the applicability of LEM.

5.1.2 Laser and dry etching combined method

Similar to wet etching, RIE tends to exhibit isotropic behavior at high working pressures and low bias power, as chemical sputtering becomes the dominant mechanism under these conditions. The combination of laser and dry etching exploits the tendency of laser-modified regions to evolve into concave spherical surfaces during dry etching, making it effective for fabricating MLAs. As shown in Fig. 9(a), Liu et al. [55] proposed a dry etching-assisted femtosecond laser machining method that consists of three stages: laser irradiation to generate the modified area, an initial etching stage targeting the modified region, and a stable etching stage to expand the dimples. This approach has been successfully employed to fabricate MLAs on Si (Fig. 9(b)). Its application has been extended to DCMs such as SiC, sapphire, GaAs, and diamond [129], as well as to the fabrication of compound eyes [130] (Fig. 9(c)).

5.2 Cutting and etching combined method

Ultra-precision machining is an advanced technology for fabricating micro- and nanostructures using single-point diamond tools. This technique is distinguished by its ability to achieve surfaces with nanometer-level precision, often eliminating the need for additional

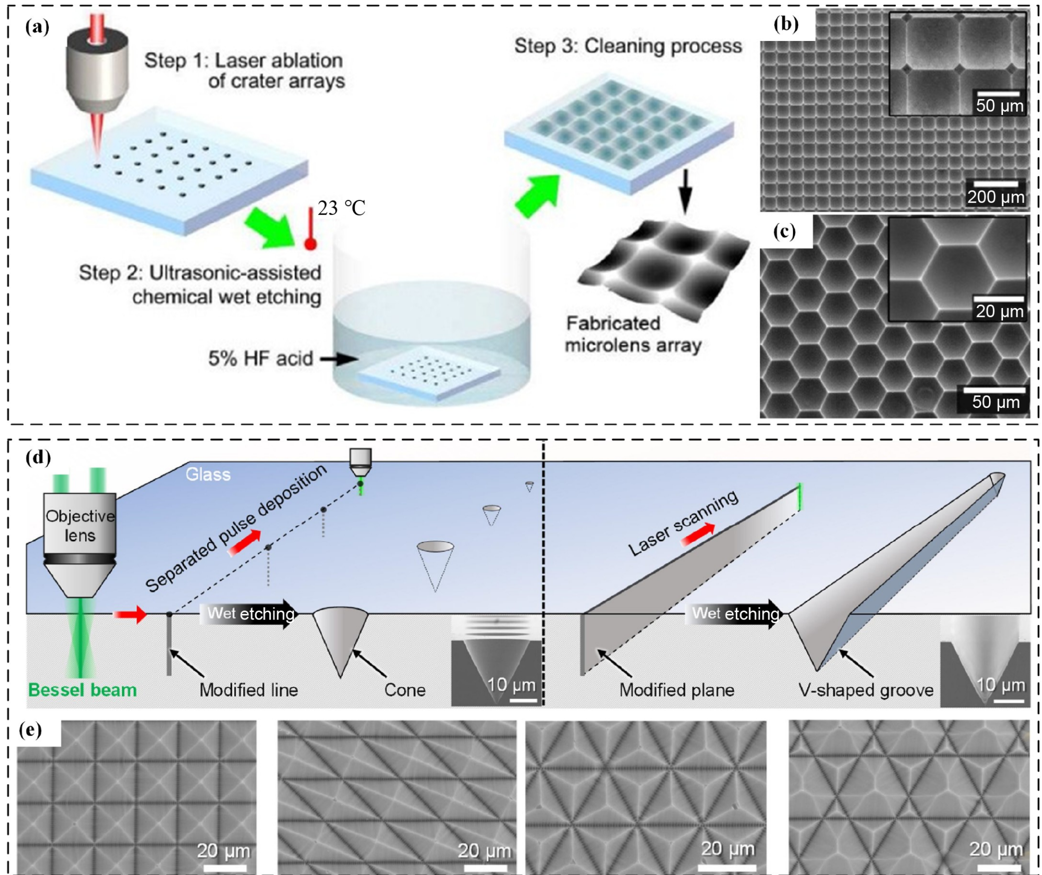

Fig. 8 MNFS fabricated by laser and wet etching combined method. (a) Schematic of femtosecond-laser-enhanced local wet etching method for (b) rectangular MLA and (c) hexagonal MLA [56]. (d) Schematic of laser-guided anisotropic etching for (e) various microstructures [32]. Reproduced from [56] with permission from Optica Publishing Group. Reproduced from [32] with permission from Elsevier.

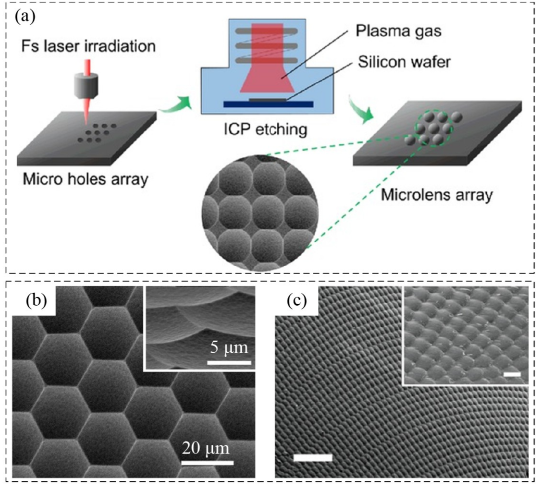

Fig. 9 MNFS fabricated using dry etching and laser combined method. (a) Schematic of laser and dry etching combined method for (b) MLAs [55] and (c) artificial compound eyes [130]. Scale bars: 100 μm for subfigure (c) and 20 μm for its inset image. Reproduced from [55] with permission from John Wiley & Sons. Reproduced from [130] with permission from John Wiley & Sons.

processing steps. It features high accuracy and versatility, making it a prevalent method for the fabrication of microstructures [131]. Various ultra-precision cutting techniques, such as single-point diamond turning, single-point diamond milling, fly cutting, and vibration-assisted cutting, are widely employed for the production of MLAs [53], micro-groove arrays [132], micropyramid arrays [29], Fresnel structures [133], and numerous other hierarchical structures [64,65].

CEM merges the flexibility of micro-cutting with the material adaptability and precision of etching, offering an advanced solution for the high-precision fabrication of MNFSs from DCMs. The overall process is divided into three stages: preparation of the coating layer, ultra-precision machining of the coating, and pattern transfer via etching. This method enables the transformation of hard and brittle materials into machinable substances such as aluminum and photoresist. The etched pattern is transferred onto the substrate of the hard and brittle material, facilitating the ultra-precision fabrication of microstructures on these materials.

We proposed a strategy that combines micro-cutting and etching for fabricating microstructures on SiC as illustrated in Fig. 10. Initially, thin films of SU-8 photoresist were created using spin coating, followed by single-point diamond machining to fabricate an MLA structure on the photoresist film. The pattern was then transferred to the SiC mold substrate using ICP etching [85] (Fig. 10(b)). However, due to the poor machinability of photoresist, achieving ultra-precision machining for

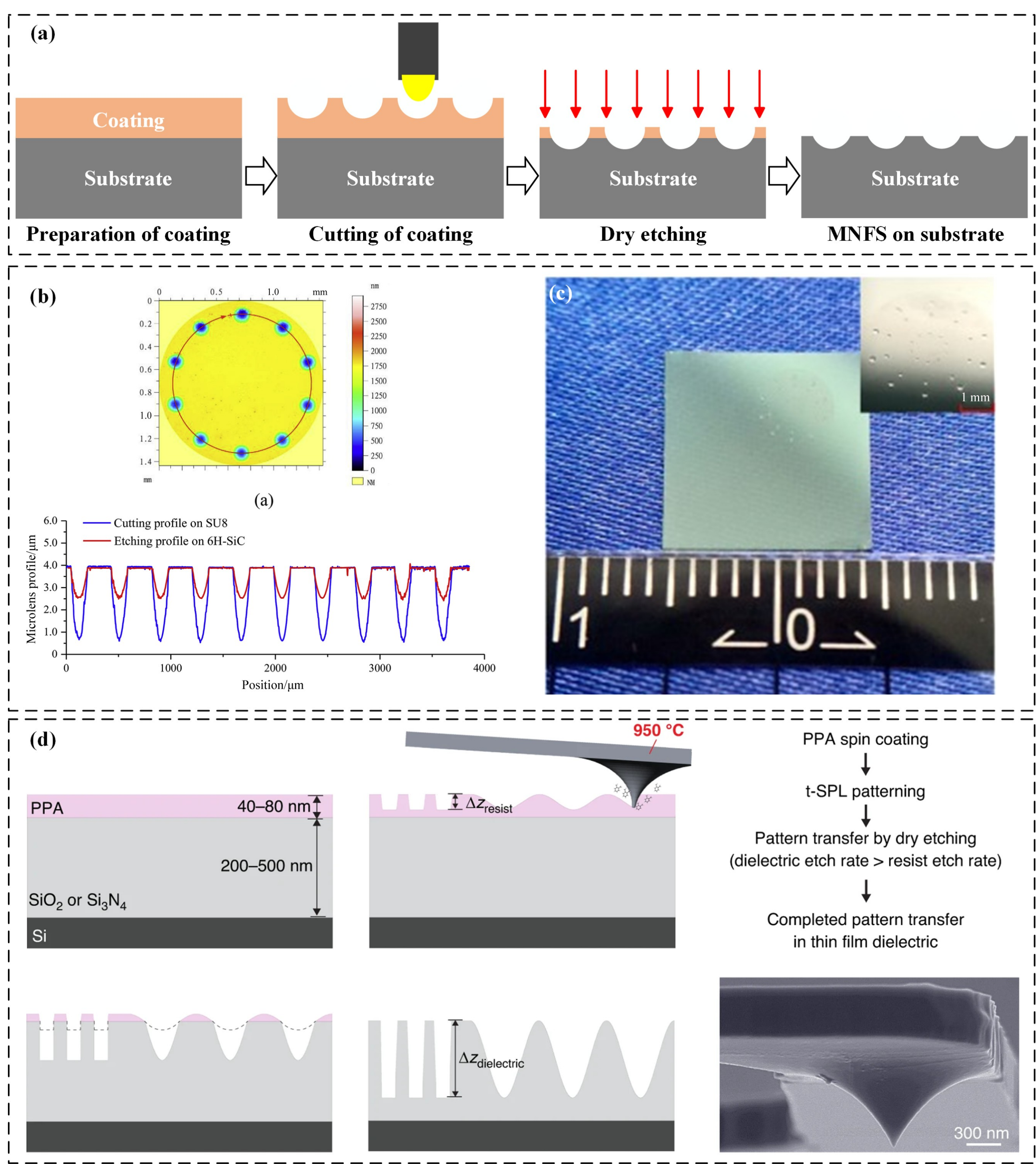

Fig. 10 MNFS fabricated using CEM. (a) Schematic of the combined cutting and etching strategy. (b) SiC MLAs processed through CEM using ICP etching [85] and (c) IBE etching [86]. (d) Combined thermal scanning probe and dry etching for grayscale nanopattern amplification [135]. Reproduced from [85] with permission from Elsevier. Reproduced from [86] with permission from Elsevier. Reproduced from [135] under CC BY 4.0 license.

the mask presents a significant challenge [134]. To further enhance precision, we employed aluminum, which exhibits superior machinability, as the coating material. An aluminum coating was applied to a 6H-SiC substrate using magnetron sputtering. A concave MLA was subsequently fabricated on the aluminum coating through servo machining using a single-point diamond slow tool and ultimately transferred onto the substrate via IBE to obtain the concave MLA mold as illustrated in Fig. 10(c) [86]. Following a similar mechanical scribing principle, Erbas et al. [135] developed a technique that integrates thermal scanning probe lithography with dry etching and achieved the isotropic amplification of nanostructures on quartz substrates as illustrated in Fig. 10(d).

5.3 Molding and etching combined method

Imprint lithography is a molding technique that transfers patterns from a mold onto polymers or photoresists through contact imprinting [136]. This method circumvents the resolution limits imposed by diffraction in optical lithography and addresses the flexibility challenges associated with two-dimensional patterning, offering ultra-high resolution, high efficiency, and low cost. Imprint lithography has been widely employed in the fabrication of various complex microstructures [137]. However, its application is primarily constrained to photosensitive materials such as photoresist and thermoplastic polymers, which significantly limits its broad applicability. In addition, this technique encounters substantial challenges when processing hard and brittle materials, including glass, Si, and SiC.

MEM involves the construction of a patterned mask structure on a film surface using imprinting techniques, followed by etching to transfer the 2.5D structure into the substrate material, as illustrated in Fig. 11(a). This technique was initially employed for the fabrication of micro-optical components, such as gratings, on fused quartz [138,139]. Through a series of optimizations, it was further applied to the fabrication of Fresnel lens structures in quartz [140]. Park et al. [82] utilized ultra-precision machining to create nickel templates as molds (Fig. 11(b)), which were then treated to prevent adhesion. They subsequently employed ICP etching to transfer the patterned mask from the photoresist to the Si substrate, successfully fabricating a spherical MLA. To enhance adaptability, our team [74,75] used polydimethylsiloxane (PDMS) as an intermediate mold and successfully fabricated microgroove arrays on SiC substrates. As a flexible composite mold, PDMS significantly improves imprint accuracy and enables the fabrication of micro-groove arrays on curved surfaces as shown in Fig. 11(c).

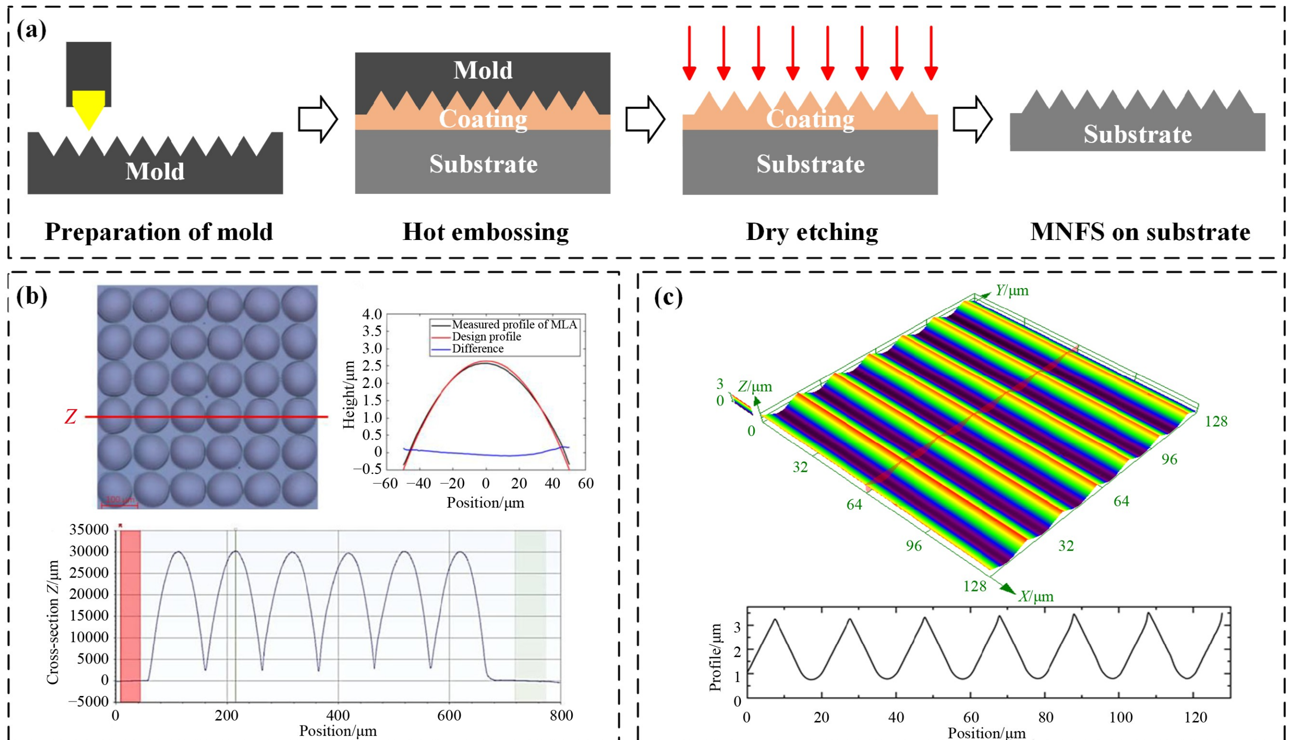

Fig. 11 MNFS fabricated using MEM. (a) Schematic of MEM strategy. (b) SiC microgroove array fabricated by MEM. (c) Si MLAs fabricated using MEM [82]. Reproduced under CC BY 4.0 license.

5.4 Self-assembly and etching combined method

SAEM involves generating mask structures through self-assembly methods, including micro/nanosphere and AAO template self-assembly. Dry etching is then employed to transfer nanometer- or micrometer-scale patterns onto the substrate [141]. This technique utilizes a monolayer of nanosphere arrays as the mask. A range of micrometer- and nanometer-scale array structures, including micro/nano pillar arrays [81], pore arrays [142], pillar/cone arrays [82], and nanowire arrays [143], are fabricated by employing various etching gases and colloidal spheres composed of polystyrene (PS) and silica (Fig. 12). Yang et al. [68] assembled a layer of smaller colloidal particles onto a monolayer of larger colloidal particles and utilized dry etching to fabricate complex hierarchical structures as shown in Fig. 13(d). In contrast to the self-assembled micro/nanosphere mask, Li et al. [40] fabricated various nanopore and nanoparticle arrays using a high-aspect-ratio AAO mask as depicted in Fig. 13.

Compared with traditional techniques that use self-assembled microspheres as mask structures, our team developed a novel SAEM strategy that utilizes microsphere self-assembly to create a photoresist dimple array mask. We utilized gas–liquid interface microsphere self-assembly to form a patterned mask on the surface of photoresist. This mask was subsequently transferred to a SiC substrate through ICP etching for MLA fabrication [91]. This approach enables the efficient and high-precision manufacturing of large-area, small-sized MLAs. However, due to the dependence on capillary forces, the arrangement of the microlenses is limited to a hexagonal pattern, which significantly restricts the method's flexibility. To address this limitation and enhance the flexibility of MLA arrangements, we introduced a template-oriented-assembly microsphere lithography method shown in Fig. 14. This technique leverages the flexible design of concave micropyramid array templates and van der Waals force-driven self-assembly to enable the controlled fabrication of MLAs with various arrangements [92].

Compared with traditional lithography, HEM presents a flexible and efficient approach for

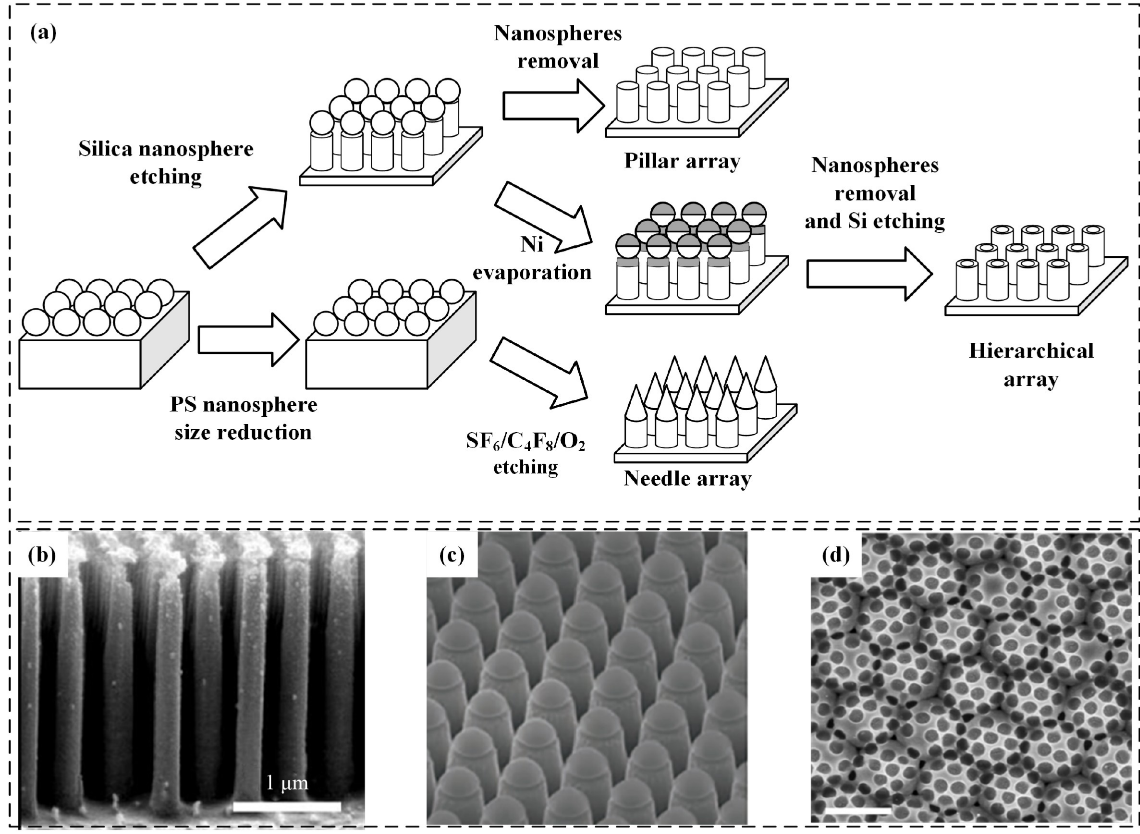

Fig. 12 MNFS fabricated using hybrid machining strategies that combine nanosphere self-assembly and etching: (a) Schematic of nanosphere lithography strategy. (b) Fabricated pillar array [81], (c) needle array [82], and (d) hierarchical array [68] on Si wafer produced through this strategy. Scale bar in subfigure (d) represents 2 μm. Reproduced from [81] with permission from IOP Publishing. Reproduced from [82] with permission from John Wiley & Sons. Reprinted from [68] with permission from John Wiley & Sons.

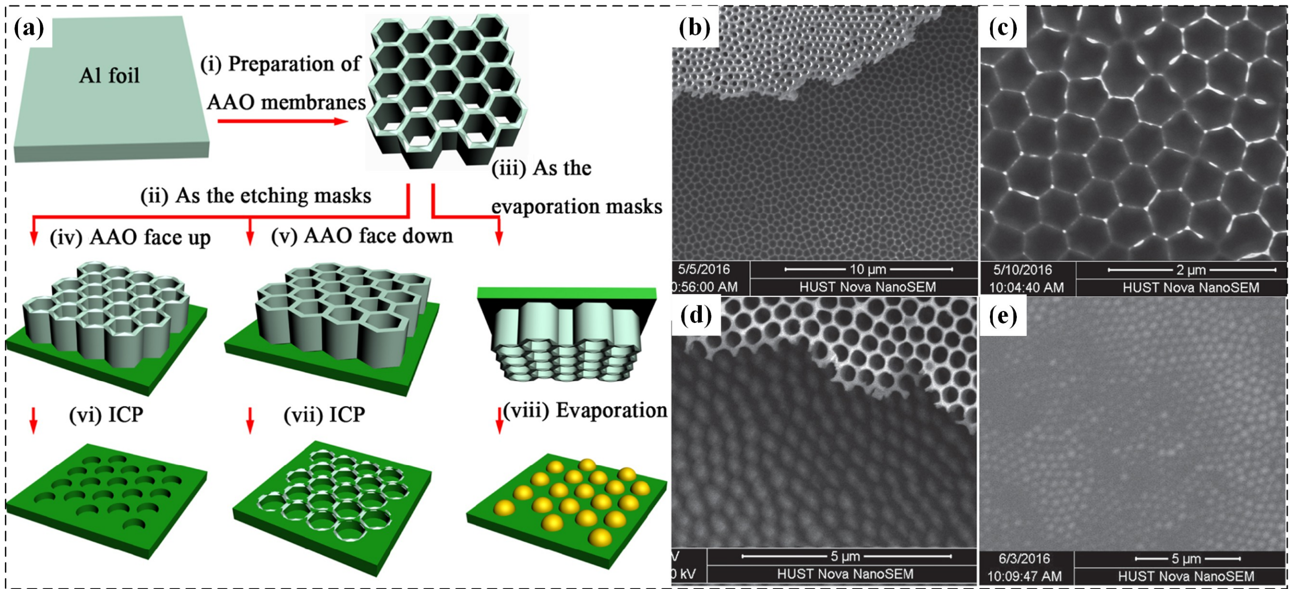

Fig. 13 MNFS fabricated by AAO template self-assembly and etching hybrid machining strategy: (a) Schematic of AAO template self-assembly and etching hybrid machining strategy. (b) Fabricated nanopore arrays on Si substrate and (c) GaN substrate. (d) Fabricated Au nanoparticle arrays on Si substrate. (e) Fabricated Cr nanoparticle arrays on Si substrate [40]. Reproduced under CC BY 4.0 license.

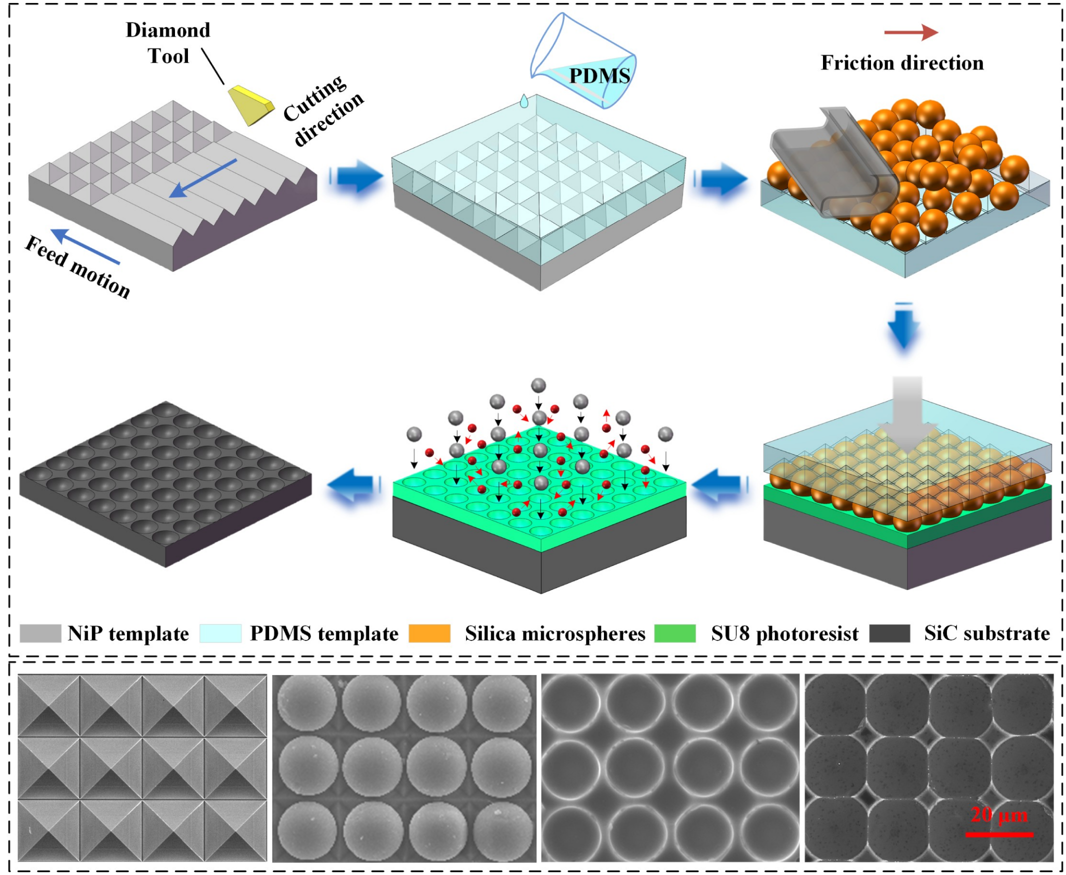

Fig. 14 Schematic of SiC MLA fabrication using template-oriented-assembly microsphere lithography.

fabricating MNFSs on DCMs and utilizes complex mask patterning and pattern transfer from heterogeneous materials through plasma etching. A detailed analysis and comparison of various HEM strategies, including LEM, CEM, MEM, and SAEM, against traditional lithography are presented in Table 2. In the future, high-precision and high-efficiency HEM strategies are poised to become the emerging trend in MNFS manufacturing on DCMs.

6 Summary and outlook

MNFSs have emerged as a significant and rapidly advancing field in materials science and engineering. This review highlights recent advancements in the theoretical foundations, fabrication strategies, and practical applications of HEM for MNFS fabrication. We analyze and compare typical forms of MNFSs in terms of functional surface characteristics and provide a comprehensive overview of HEM strategies for MNFS fabrication on DCMs. We also discuss the current state of development in the modeling and simulation of etching pattern transfer, emphasizing precision control during this process. Despite the considerable advancements in HEM strategies in recent years, several challenges persist and are listed as follows:

- Many researchers utilized biomimicry to design and fabricate MNFSs for specific functions. Despite the availability of numerous high-performance examples, the fabrication of these MNFSs, particularly hierarchical MNFSs, presents a significant challenge.
- A primary challenge in HEM strategies is the large-scale fabrication of complex mask structures with high precision, consistency, and efficiency. Advanced mask patterning and hybrid processing techniques must be developed to address the increasing complexity of MNFSs.
- Another critical challenge involves developing mathematical models that accurately map the geometric relationships between mask and substrate structures and simulating the transfer mechanisms of complex 3D shapes during pattern transfer. Further work is required to enhance the modeling and simulation of complex 3D structures in homogeneous and heterogeneous materials.

Looking ahead, HEM strategies are expected to play a crucial role in advancing the production of MNFSs with extreme characteristics, such as large areas, high precision, cross-scale features, and complex shapes. In terms of functional applications, single-function structures are becoming increasingly inadequate, whereas multifunctional, integrated, multi-scale periodic structure arrays are receiving growing interest. The development of these multifunctional and layered multi-scale periodic structure arrays with significant functional advantages is an inevitable trend for future advancements.

Nomenclature

Abbreviations

AAO	Anodic aluminum oxide
CEM	Cutting and etching combined machining
DCM	Difficult-to-cut material
HEM	Hybrid etching machining
IBE	Ion beam etching
ICP	Inductively coupled plasma
IEAD	Ion energy and angular distribution
LEM	Laser and etching combined machining
LGAE	Laser-guided anisotropic etching
MEM	Molding and etching combined machining
MLA	Microlens array

Table 2 Overview of various etching-assisted hybrid strategies for MNFS fabrication[a)]

Strategies	Precision	Efficiency	Structure flexibility	Scale flexibility
Assisted etching				
UV lithography	☆☆☆	☆☆☆☆	☆☆☆	☆☆☆
Grayscale lithography	☆☆	☆☆☆	☆☆☆☆☆	☆☆☆☆
Thermal reflow	☆☆☆☆☆	☆☆☆☆	☆☆	☆☆☆
Others				
LEM	☆☆☆☆	☆☆☆	☆☆	☆☆☆
CEM	☆☆☆	☆☆☆	☆☆☆☆	☆☆☆☆
MEM	☆☆☆☆	☆☆☆☆☆	☆☆☆☆☆	☆☆☆☆☆
SAEM	☆☆☆☆	☆☆☆☆☆	☆☆☆	☆☆☆☆☆

a) More stars indicate superior performance.

MNFS	Micro/nano functional structure
PDMS	Polydimethylsiloxane
PS	Polystyrene
RIE	Reactive ion etching
SAEM	Self-assembly and etching combined machining
UV	Ultraviolet

Acknowledgements The authors gratefully acknowledge the financial supports by the National Natural Science Foundation of China (Grant Nos.52435008, 52205440, and 52205441).

Conflict of Interest The authors declare no conflict of interest.

Open Access This article is licensed under a Creative Commons Attribution 4.0 International License, which permits use, sharing, adaptation, distribution, and reproduction in any medium or format, as long as appropriate credit is given to the original author(s) and source, a link to the Creative Commons license is provided, and the changes made are indicated.

The images or other third-party material in this article are included in the article's Creative Commons license, unless indicated otherwise in a credit line to the material. If material is not included in the article's Creative Commons license and your intended use is not permitted by statutory regulation or exceeds the permitted use, you will need to obtain permission directly from the copyright holder.

Visit https://creativecommons.org/licenses/by/4.0/ to view a copy of this license.

References

1. Dyck O, Jesse S, Delby N, Kalinin S V, Lupini A R. Variable voltage electron microscopy: Toward atom-by-atom fabrication in 2D materials. Ultramicroscopy, 2020, 211: 112949
2. Jeong S J, Xia G D, Kim B H, Shin D H, Kwon S H, Kang S W, Kim S O. Universal block copolymer lithography for metals, semiconductors, ceramics, and polymers. Advanced Materials, 2008, 20(10): 1898–1904
3. Liu X, Ding C L, Gao X J, Shen X M, Tang M B, Yang Z Y, Xu L, Kuang C F, Liu X. High-resolution 3D nanoprinting based on two-step absorption via an integrated fiber-coupled laser diode. Optics Letters, 2023, 48(16): 4300–4303
4. Zhang Y P, Le Friec A, Chen M L. 3D anisotropic conductive fibers electrically stimulated myogenesis. International Journal of Pharmaceutics, 2021, 606: 120841
5. Song M W, Feng L, Huo P C, Liu M Z, Huang C Y, Yan F, Lu Y Q, Xu T. Versatile full-colour nanopainting enabled by a pixelated plasmonic metasurface. Nature Nanotechnology, 2023, 18(1): 71–78
6. Xia R, Li Y, You S, Lu C H, Xu W B, Ni Y R. Asymmetric plasmonic moth-eye nanoarrays with side opening for broadband incident-angle-insensitive antireflection and absorption. Materials, 2023, 16(17): 5988
7. Bhushan B, Jung Y C. Natural and biomimetic artificial surfaces for superhydrophobicity, self-cleaning, low adhesion, and drag reduction. Progress in Materials Science, 2011, 56(1): 1–108
8. Hirai Y, Okuda N, Saito N, Ogawa T, Machida R, Nomura S, Ôhara M, Haseyama M, Shimomura M. The friction properties of firebrat scales. Biomimetics, 2019, 4(1): 2
9. Bian Y M, Cao L, Zeng D H, Cui J, Li W, Yu Z T, Zhang P. The tribological properties of two-phase hard and soft composite wear-resistant coatings on titanium alloys. Surface and Coatings Technology, 2023, 456: 129256
10. Pan R, Zhang H J, Zhong M L. Triple-scale superhydrophobic surface with excellent anti-icing and icephobic performance via ultrafast laser hybrid fabrication. ACS Applied Materials & Interfaces, 2021, 13(1): 1743–1753
11. Dhyani A, Choi W, Golovin K, Tuteja A. Surface design strategies for mitigating ice and snow accretion. Matter, 2022, 5(5): 1423–1454
12. Wang B, Liang W X, Guo Z G, Liu W M. Biomimetic super-lyophobic and super-lyophilic materials applied for oil/water separation: a new strategy beyond nature. Chemical Society Reviews, 2015, 44(1): 336–361
13. Liu W J, Pan R, Cai M Y, Luo X, Chen C H, Jiang G C, Hu X Y, Zhang H J, Zhong M L. Oil-triggered switchable wettability on patterned alternating air/lubricant-infused superamphiphobic surfaces. Journal of Materials Chemistry A, 2020, 8(14): 6647–6660
14. Wang D H, Sun Q Q, Hokkanen M J, Zhang C L, Lin F Y, Liu Q, Zhu S P, Zhou T F, Chang Q, He B, Zhou Q, Chen L Q, Wang Z K, Ras R H A, Deng X. Design of robust superhydrophobic surfaces. Nature, 2020, 582(7810): 55–59
15. Yue C, Yu Y J, Wu Z G, Sun S B, He X, Li J T, Zhao L B, Wu S T, Li J, Kang J Y, Lin L W. High stability induced by the TiN/Ti interlayer in three-dimensional Si/Ge nanorod arrays as anode in micro lithium ion battery. ACS Applied Materials & Interfaces, 2016, 8(12): 7806–7810
16. Xu L Y, Wang Z L, Song Q, Sun X H, Liu H Y, Fang R C, Jiang X Y. Microstructures formation through liquid-assisted assembly of functional materials for high-performance electronics. Advanced Functional Materials, 2024, 34(17): 2315162
17. Song L J, Sun L W, Zhao J, Wang X H, Yin J H, Luan S F, Ming W H. Synergistic superhydrophobic and photodynamic cotton textiles with remarkable antibacterial activities. ACS Applied Bio Materials, 2019, 2(7): 2756–2765
18. Dalby M J, Gadegaard N, Oreffo R O C. Harnessing

nanotopography and integrin–matrix interactions to influence stem cell fate. Nature Materials, 2014, 13(6): 558–569
19. Zhang Z Y, Yan J W, Kuriyagawa T. Manufacturing technologies toward extreme precision. International Journal of Extreme Manufacturing, 2019, 1(2): 022001
20. Fang F Z, Zhang N, Guo D M, Ehmann K, Cheung B, Liu K, Yamamura K. Towards atomic and close-to-atomic scale manufacturing. International Journal of Extreme Manufacturing, 2019, 1(1): 012001
21. Liu H G, Lin W X, Hong M H. Hybrid laser precision engineering of transparent hard materials: challenges, solutions and applications. Light: Science & Applications, 2021, 10(1): 162
22. Bellotti M, De Eguilior Caballero J R, Qian J, Reynaerts D. Effects of partial tool engagement in micro-EDM milling and adaptive tool wear compensation strategy for efficient milling of inclined surfaces. Journal of Materials Processing Technology, 2021, 288: 116852
23. Pease R F, Chou S Y. Lithography and other patterning techniques for future electronics. Proceedings of the IEEE, 2008, 96(2): 248–270
24. Bixler G D, Bhushan B. Bioinspired rice leaf and butterfly wing surface structures combining shark skin and lotus effects. Soft Matter, 2012, 8(44): 11271–11284
25. Lee J H, Park S R, Yang S H, Kim Y S. Fabrication of a V-groove on the optical fiber connector using a miniaturized machine tool. Journal of Materials Processing Technology, 2004, 155–156: 1716–1722
26. He Y P, Zhou T F, Ning Y W, Hu Y, Yu Q, Zhao W X, Wang X B, Kumar A S. Three-level nanogrooves by vibration-assisted fly-cutting for diffraction regulation and array output. Optics Letters, 2022, 47(11): 2730–2733
27. Li C J, Fang Y C, Chu W T, Cheng M C. Design of a prism light-guide plate for an LCD backlight module. Journal of the Society for Information Display, 2008, 16(4): 545–550
28. Kumar M D, Kim H, Kim J. Periodically patterned Si pyramids for realizing high efficient solar cells by wet etching process. Solar Energy, 2015, 117: 180–186
29. Dong X B, Zhou T F, Pang S Q, Liang Z Q, Yu Q, Ruan B S, Wang X B. Comparison of fly cutting and transverse planing for micropyramid array machining on nickel phosphorus plating. The International Journal of Advanced Manufacturing Technology, 2019, 102(5–8): 2481–2489
30. Garcell E M, Guo C L. Polarization-controlled microgroove arrays induced by femtosecond laser pulses. Journal of Applied Physics, 2018, 123(21): 213103
31. Zhang R, Huang C Z, Wang J, Zhu H T, Yao P, Feng S C. Micromachining of 4H-SiC using femtosecond laser. Ceramics International, 2018, 44(15): 17775–17783
32. Li J, Zhong S, Huang J X, Qiu P, Wang P, Li H, Qin C, Miao D, Xu S L. Laser-guided anisotropic etching for precision machining of micro-engineered glass components. International Journal of Machine Tools and Manufacture, 2024, 198: 104152
33. Vanthanh K, Ma Y C, Si J H, Chen T, Chen F, Hou X. Fabrication of micro-grooves in silicon carbide using femtosecond laser irradiation and acid etching. Chinese Physics Letters, 2014, 31(3): 037901
34. Ng H M, Weimann N G, Chowdhury A. GaN nanotip pyramids formed by anisotropic etching. Journal of Applied Physics, 2003, 94(1): 650–653
35. Zhu B, Cao H, Chen Z X, Wang W T, Shi Z K, Xiao K J, Lei Y F, Liu S, Song Y, Xue L J. Bioinspired micropillar array with micropit for robust and strong adhesion. Chemical Engineering Journal, 2023, 454: 140227
36. Søndergaard T, Novikov S M, Holmgaard T, Eriksen R L, Beermann J, Han Z H, Pedersen K, Bozhevolnyi S I. Plasmonic black gold by adiabatic nanofocusing and absorption of light in ultra-sharp convex grooves. Nature Communications, 2012, 3(1): 969
37. Seo S W, Song Y, Mustakim N. Hydrogel micropillar array for temperature sensing in fluid. IEEE Sensors Journal, 2023, 23(17): 19021–19027
38. He B, Tait N, Regnier F. Fabrication of nanocolumns for liquid chromatography. Analytical Chemistry, 1998, 70(18): 3790–3797
39. Li J, Hu Y X, Yu L, Li L, Ji D Y, Li L Q, Hu W P, Fuchs H. Recent advances of nanospheres lithography in organic electronics. Small, 2021, 17(28): 2100724
40. Li Z P, Xu Z M, Qu X P, Wang S B, Peng J, Mei L H. Fabrication of nanopore and nanoparticle arrays with high aspect ratio AAO masks. Nanotechnology, 2017, 28(9): 095301
41. Riedl J, Ding Y, Fleming A M, Burrows C J. Identification of DNA lesions using a third base pair for amplification and nanopore sequencing. Nature Communications, 2015, 6(1): 8807
42. Lee H S, Suk J, Kim H, Kim J, Song J, Jeong D S, Park J K, Kim W M, Lee D K, Choi K J, Ju B K, Lee T S, Kim I. Enhanced efficiency of crystalline Si solar cells based on kerfless-thin wafers with nanohole arrays. Scientific Reports, 2018, 8(1): 3504
43. Mahigir A, Chang T W, Behnam A, Liu G L, Gartia M R, Veronis G. Plasmonic nanohole array for enhancing the SERS signal of a single layer of graphene in water. Scientific Reports, 2017, 7(1): 14044
44. Jain M, Koren S, Miga K H, Quick J, Rand A C, Sasani T A, Tyson J R, Beggs A D, Dilthey A T, Fiddes I T, Malla S, Marriott H, Nieto T, O'Grady J, Olsen H E, Pedersen B S, Rhie A, Richardson H, Quinlan A R, Snutch T P, Tee L, Paten B, Phillippy A M, Simpson J T, Loman N J, Loose M. Nanopore

sequencing and assembly of a human genome with ultra-long reads. Nature Biotechnology, 2018, 36(4): 338–345

45. Li X X, Qin X, Wang Z, Wu Y F, Wang K, Xia X H, Liu S Q. *In situ* imaging of endogenous hydrogen peroxide efflux from living cells via bipolar gold nanoelectrode array and electrochemiluminescence technology. ACS Sensors, 2022, 7(8): 2446–2453
46. Tu S B, Chen Z H, Zhang B, Wang X C, Zhan R M, Li C H, Sun Y M. Realizing high utilization of high-mass-loading sulfur cathode via electrode nanopore regulation. Nano Letters, 2022, 22(14): 5982–5989
47. Deng Q M, Cao Y Q, Wan X F, Wang B, Sun A M, Wang H Z, Wang Y F, Wang H Z, Gu H C. Nanopore-based metagenomic sequencing for the rapid and precise detection of pathogens among immunocompromised cancer patients with suspected infections. Frontiers in Cellular and Infection Microbiology, 2022, 12: 943859
48. Wen T L, Booth R A, Majetich S A. Ten-nanometer dense hole Arrays generated by nanoparticle lithography. Nano Letters, 2012, 12(11): 5873–5878
49. Stępniowski W J, Durejko T, Michalska-Domańska M, Łazińska M, Aniszewska J. Characterization of nanoporous anodic aluminum oxide formed on laser pre-treated aluminum. Materials Characterization, 2016, 122: 130–136
50. Wang T X, Cheng X Y, Li X, Ma J, Yan S, Hu X L, Qi K, Fan W W, Liu M M, Xu X, Lu X Y, Jiang X M, Zhang Y. Femtosecond-laser-assisted high-aspect-ratio nanolithography in lithium niobate. Nanoscale, 2023, 15(37): 15298–15303
51. Zhang X F, Yao Z Q, Hou Z B, Song J C. Processing and profile control of microhole array for PDMS mask with femtosecond laser. Micromachines, 2022, 13(2): 340
52. Zhou W C, Raasch T W, Yi A Y. Design, fabrication, and testing of a Shack–Hartmann sensor with an automatic registration feature. Applied Optics, 2016, 55(28): 7892–7899
53. Zhou T F, Zhang Z Q, Zhou J, Zhao B, Yao X Q, Wang X B, Hu J J, Zeng J Y. Study of quadrifoliate tool-setting method for diamond milling of microlens array. Precision Engineering, 2023, 83: 170–180
54. Zhang Z Q, Zhou T F, Zhao B, Yao X Q, Zeng J Y. Study of integrated milling-grinding of microlens array on binderless tungsten carbide with diamond grains ball-end tool. Precision Engineering, 2024, 88: 540–548
55. Liu X Q, Chen Q D, Guan K M, Ma Z C, Yu Y H, Li Q K, Tian Z N, Sun H B. Dry-etching-assisted femtosecond laser machining. Laser & Photonics Reviews, 2017, 11(3): 1600115
56. Chen F, Liu H W, Yang Q, Wang X H, Hou C, Bian H, Liang W W, Si J H, Hou X. Maskless fabrication of concave microlens arrays on silica glasses by a femtosecond-laser-enhanced local wet etching method. Optics Express, 2010, 18(19): 20334–20343
57. Zhou W J, Li R, Li M, Tao P, Wang X S, Dai S X, Song B A, Zhang W, Lin C G, Shen X, Xu T F, Zhang P Q. Fabrication of microlens array on chalcogenide glass by wet etching-assisted femtosecond laser direct writing. Ceramics International, 2022, 48(13): 18983–18988
58. Zhang H, Ding B, Chen T H. A high efficiency industrial polysilicon solar cell with a honeycomb-like surface fabricated by wet etching using a photoresist mask. Applied Surface Science, 2016, 387: 1265–1273
59. Lee H Y, Kim D W, Sung Y J, Yeom G Y. Fabrication of SiC micro-lens by plasma etching. Thin Solid Films, 2005, 475(1–2): 318–322
60. Savander P. Microlens arrays etched into glass and silicon. Optics and Lasers in Engineering, 1994, 20(2): 97–107
61. Suleski T J, O’Shea D C. Gray-scale masks for diffractive-optics fabrication: I. Commercial slide imagers. Applied Optics, 1995, 34(32): 7507–7517
62. Guo Q, Ma J Y, Yin T J, Jin H C, Zheng J X, Gao H. Superhydrophobic non-metallic surfaces with multiscale nano/micro-structure: fabrication and application. Molecules, 2024, 29(9): 2098
63. Fu Y Q, Liu Y, Zhou X L, Xu Z W, Fang F Z. Experimental investigation of superfocusing of plasmonic lens with chirped circular nanoslits. Optics Express, 2010, 18(4): 3438–3443
64. Zhu Z W, To S, Zhang S J. Theoretical and experimental investigation on the novel end-fly-cutting-servo diamond machining of hierarchical micro-nanostructures. International Journal of Machine Tools and Manufacture, 2015, 94: 15–25
65. He Y P, Zhou T F, Dong X B, Liu P, Zhao W X, Wang X B, Hu Y, Yan J W. Generation of high-saturation two-level iridescent structures by vibration-assisted fly cutting. Materials & Design, 2020, 193: 108839
66. Hu J, Xu K, Huang P L, Wang M, Xu S L, Wei Q H. Hierarchical conical metasurfaces as ultra-broadband perfect absorbers from visible to far-infrared regime. Advanced Functional Materials, 2024, 34(6): 2309229
67. Zhang L S, Uzoma P C, Chu X Y, Penkov O V, Hu H. Bio-inspired hierarchical micro/nanostructured surfaces for superhydrophobic and anti-ice applications. Frontiers in Bioengineering and Biotechnology, 2022, 10: 872268
68. Yang S K, Sun N, Stogin B B, Wang J, Huang Y, Wong T S. Ultra-antireflective synthetic brochosomes. Nature Communications, 2017, 8(1): 1285
69. Wang L L, Deng Y, Zou Z X, Xiao Y J, Su G K, Guo Z N. Microgroove formation in thin copper by laser-induced cavitation bubble shock: numerical and experimental investigation. Applied Optics, 2022, 61(8): 1841–1850
70. Zhang M C, Lee Y, Zheng Z Q, Khan M T A, Lyu X

L, Byun J, Giessen H, Sitti M. Micro- and nanofabrication of dynamic hydrogels with multichannel information. Nature Communications, 2023, 14(1): 8208

71. Chen S S, Yang S M, Cheung C F, Duan D Z, Ho L T, Jiang Z D, Kang C W. Fabrication of the high-precision micro-structure array using a phase shift modulation of superimposed oscillation in ultra-precision grinding. Optics Express, 2022, 30(24): 44321–44338
72. Ma S Y, Lu Y J, Fu Y F, Li X H, Lai J J, Zhang J G, Chen X, Xiao J F, Xu J F. Investigation on the machinability of polycrystalline ZnSe by elliptical vibration diamond cutting. Optics Express, 2024, 32(1): 482–498
73. Jing X F, Shao J D, Zhang J C, Jin Y X, He H B, Fan Z X. Calculation of femtosecond pulse laser induced damage threshold for broadband antireflective microstructure arrays. Optics Express, 2009, 17(26): 24137–24152
74. Yao X Q, Zhou T F, Su X B, Guo W J, Liu P, Yu Q, Zhao B, Zeng J Y. Modeling of surface evolution in plasma etching for SiC microgroove fabrication. Ceramics International, 2024, 50(17): 30504–30513
75. Yao X Q, Zhou T F, Su X B, Wang G, Guo W J, Yang X Z, Zhao B, Wang X B. Research on wafer-level SiC microgroove array process via integrated molding-etching process. Journal of Materials Processing Technology, 2024, 334: 118645
76. Hwang S, Lim K, Shin H, Lee S, Jang M. Micro-pyramidal structure fabrication on polydimethyl-siloxane (PDMS) by Si (100) KOH wet etching. Journal of the Korean Physical Society, 2017, 71(8): 506–509
77. Ding K, Zhang M, Mao J, Xiao P, Zhang X W, Wu D, Zhang X J, Jie J S. High-resolution image patterned silicon wafer with inverted pyramid micro-structure arrays for decorative solar cells. Materials Today Energy, 2020, 18: 100493
78. Frost W, Carpenter R, Couet S, O'Grady K, Vallejo Fernandez G. Distributions of easy axes and reversal processes in patterned MRAM arrays. Scientific Reports, 2023, 13(1): 20490
79. Gierse M, Marshall A, Qureshi M U, Scharpf J, Parker A J, Hausmann B J M, Walther P, Bleszynski Jayich A C, Jelezko F, Neumann P, Schwartz I. Scalable and tunable diamond nanostructuring process for nanoscale NMR applications. ACS Omega, 2022, 7(35): 31544–31550
80. Huh J. Directed self-assembly of cylinder-forming block copolymers using pillar topographic patterns. Polymers, 2024, 16(7): 881
81. Cheung C L, Nikolić R J, Reinhardt C E, Wang T F. Fabrication of nanopillars by nanosphere lithography. Nanotechnology, 2006, 17(5): 1339
82. Park H, Shin D, Kang G, Baek S, Kim K, Padilla W J. Broadband optical antireflection enhancement by integrating antireflective nanoislands with silicon nanoconical-frustum arrays. Advanced Materials, 2011, 23(48): 5796–5800
83. Zhou T F, Zhou J, Wang T X, Gao L H, Ruan B S, Yu Q, Zhao W X, Wang X B. Fabrication of high aspect-ratio aspheric microlens array based on local spiral diamond milling. Journal of Manufacturing Processes, 2022, 83: 547–554
84. Sun Q Q, Tang J X, Shen L F, Lan J, Shen Z F, Xiao J F, Chen X, Zhang J G, Wu Y, Xu J F, Wang X F. Fabrication of high precision silicon spherical microlens arrays by hot embossing process. Micromachines, 2022, 13(6): 899
85. Zhou T F, Xu R Z, Ruan B S, Liang Z Q, Wang X B. Fabrication of microlens array on 6H-SiC mold by an integrated microcutting-etching process. Precision Engineering, 2018, 54: 314–320
86. Zhou T F, Xu R Z, Ruan B S, He Y P, Liang Z Q, Wang X B. Study on new method and mechanism of microcutting-etching of microlens array on 6H-SiC mold by combining single point diamond turning with ion beam etching. Journal of Materials Processing Technology, 2020, 278: 116510
87. Mu H R, Smith D, Katkus T, Gailevičius D, Malinauskas M, Nishijima Y, Stoddart P R, Ruan D, Ryu M, Morikawa J, Vasiliev T, Lozovski V, Moraru D, Ng S H, Juodkazis S. Polarisation control in arrays of microlenses and gratings: performance in visible–IR spectral ranges. Micromachines, 2023, 14(4): 798
88. Wang Q J, Yang S R, Yang Z J, Duan J, Xiong W, Deng L M. Rapid fabrication of large-area concave microlens arrays on silica glasses by femtosecond laser bursts. Optics Letters, 2022, 47(15): 3936–3939
89. Tormen M, Carpentiero A, Ferrari E, Cojoc D, Fabrizio E D. Novel fabrication method for three-dimensional nanostructuring: an application to micro-optics. Nanotechnology, 2007, 18(38): 385301
90. Larsen K P, Ravnkilde J T, Hansen O. Investigations of the isotropic etch of an ICP source for silicon microlens mold fabrication. Journal of Micromechanics and Microengineering, 2005, 15(4): 873
91. Xu R Z, Zhou T F, Cheung R. Fabrication of SiC concave microlens array mold based on microspheres self-assembly. Microelectronic Engineering, 2021, 236: 111481
92. Yao X Q, Zhou T F, Yu Q, He Y P, Su X B, Zhao B, Wang X B, Zhang Z Y. Template-oriented-assembly microsphere lithography for multi-type SiC microlens arrays. Applied Surface Science, 2024, 673: 160857
93. Goodwin M J, Harteveld C A M, de Boer M J, Vos W L. Deep reactive ion etching of cylindrical nanopores in silicon for photonic crystals. Nanotechnology, 2023, 34(22): 225301
94. Osada Y, Teshima S, Munakata H, Yanagishita T. Preparation of ordered nanohole arrays by two-step

anodization of austenitic stainless steel substrates. Langmuir, 2024, 40(34): 18338–18345
95. Petersen R S, Keller S S, Hansen O, Boisen A. Fabrication of Ni stamp with high aspect ratio, two-leveled, cylindrical microstructures using dry etching and electroplating. Journal of Micromechanics and Microengineering, 2015, 25(5): 055021
96. Tung S W, Kuo C H, Hsu L S, Yang Y J. Fabricating barbed microtip arrays by low-cost silicon wet etching techniques. In: 2013 Transducers & Eurosensors XXVII: The 17th International Conference on Solid-State Sensors, Actuators and Microsystems. Barcelona: IEEE, 2013, 1028–1031
97. Xing Y, Gosálvez M A, Zhang H, Li Y, Qiu X L. Transient and stable profiles during anisotropic wet etching of quartz. Journal of Microelectromechanical Systems, 2017, 26(5): 1063–1072
98. Suzuki K, Youn S W, Wang Q, Hiroshima H, Nishioka Y. Fabrication of sub 20-nm wide grooves in a quartz mold by space narrowing dry etching. Microelectronic Engineering, 2013, 110: 432–435
99. Murias D, Reyes-Betanzo C, Moreno M, Torres A, Itzmoyotl A, Ambrosio R, Soriano M, Lucas J, Cabarrocas P R I. Black Silicon formation using dry etching for solar cells applications. Materials Science and Engineering: B, 2012, 177(16): 1509–1513
100. Rammohan A, Dwivedi P K, Martinez-Duarte R, Katepalli H, Madou M J, Sharma A. One-step maskless grayscale lithography for the fabrication of 3-dimensional structures in SU-8. Sensors and Actuators B: Chemical, 2011, 153(1): 125–134
101. Kim J, Joy D C, Lee S Y. Controlling resist thickness and etch depth for fabrication of 3D structures in electron-beam grayscale lithography. Microelectronic Engineering, 2007, 84(12): 2859–2864
102. Aderneuer T, Fernández O, Ferrini R. Two-photon grayscale lithography for free-form micro-optical arrays. Optics Express, 2021, 29(24): 39511–39520
103. Zhang J M, Guo C F, Wang Y S, Miao J J, Tian Y, Liu Q. Micro-optical elements fabricated by metal-transparent-metallic-oxides grayscale photomasks. Applied Optics, 2012, 51(27): 6606–6611
104. Bekker C, Arshad M J, Cilibrizzi P, Nikolatos C, Lomax P, Wood G S, Cheung R, Knolle W, Ross N, Gerardot B, Bonato C. Scalable fabrication of hemispherical solid immersion lenses in silicon carbide through grayscale hard-mask lithography. Applied Physics Letters, 2023, 122(17): 173507
105. Liu X Q, Cheng R, Zheng J X, Yang S N, Wang B X, Bai B F, Chen Q D, Sun H B. Wear-resistant blazed gratings fabricated by etching-assisted femtosecond laser lithography. Journal of Lightwave Technology, 2021, 39(14): 4690–4694
106. Morgan B, Waits C M, Krizmanic J, Ghodssi R. Development of a deep silicon phase fresnel lens using gray-scale lithography and deep reactive ion etching. Journal of Microelectromechanical Systems, 2004, 13(1): 113–120
107. Khazi I, Muthiah U, Mescheder U. 3D free forms in c-Si via grayscale lithography and RIE. Microelectronic Engineering, 2018, 193: 34–40
108. Kirchner R, Schift H. Thermal reflow of polymers for innovative and smart 3D structures: A review. Materials Science in Semiconductor Processing, 2019, 92: 58–72
109. Severi M, Mottier P L. Etching selectivity control during resist pattern transfer into silica for the fabrication of microlenses with reduced spherical aberration. Optical Engineering, 1999, 38(1): 146–150
110. Liu H Y, Herrnsdorf J, Gu E, Dawson M D. Control of edge bulge evolution during photoresist reflow and its application to diamond microlens fabrication. Journal of Vacuum Science & Technology B, 2016, 34(2): 021602
111. Liang Y, Zhu T F, Xi M J, Abbasi H N, Fu J, Su R, Song Z Q, Wang H X, Wang K Y. Fabrication of a diamond concave microlens array for laser beam homogenization. Optics & Laser Technology, 2021, 136: 106738
112. Vanraes P, Parayil Venugopalan S, Besemer M, Bogaerts A. Assessing neutral transport mechanisms in aspect ratio dependent etching by means of experiments and multiscale plasma modeling. Plasma Sources Science and Technology, 2023, 32(6): 064004
113. Saleem F, Liu G Y, Liu G G, Chen B, Yun Q B, Ge Y Y, Zhang A, Wang X X, Zhou X C, Wang G, Liao L W, He Z, Li L J, Zhang H. Crystal-phase-selective etching of heterophase Au nanostructures. Small Methods, 2024, 8(11): 2400430
114. Kim H J, Wen L, Kim D S, Kim K H, Hong J W, Chang W J, Namgoong S, Kim D W, Yeom G Y. Effect of different pulse modes during Cl_2/Ar inductively coupled plasma etching on the characteristics of nanoscale silicon trench formation. Applied Surface Science, 2022, 596: 153604
115. Tuda M, Nishikawa K, Ono K. Numerical study of the etch anisotropy in low-pressure, high-density plasma etching. Journal of Applied Physics, 1997, 81(2): 960–967
116. Gottscho R A, Jurgensen C W, Vitkavage D J. Microscopic uniformity in plasma etching. Journal of Vacuum Science & Technology B, 1992, 10(5): 2133–2147
117. Winters H F. The role of chemisorption in plasma etching. Journal of Applied Physics, 1978, 49(10): 5165–5170
118. Coburn J W, Winters H F. Plasma etching—A discussion of mechanisms. Journal of Vacuum Science and Technology, 1979, 16(2): 391–403
119. Shaqfeh E S G, Jurgensen C W. Simulation of reactive ion etching pattern transfer. Journal of Applied Physics, 1989, 66(10): 4664–4675

120. Levinson J A, Shaqfeh E S G, Balooch M, Hamza A V. Ion-assisted etching and profile development of silicon in molecular and atomic chlorine. Journal of Vacuum Science & Technology B, 2000, 18(1): 172–190
121. Vyvoda M A, Li M, Graves D B, Lee H, Malyshev M V, Klemens F P, Lee J T C, Donnelly V M. Role of sidewall scattering in feature profile evolution during Cl_2 and HBr plasma etching of silicon. Journal of Vacuum Science & Technology B, 2000, 18(2): 820–833
122. Zier M, Hauffe W. Computer simulation of the topography evolution on ion bombarded surfaces. Nuclear Instruments and Methods in Physics Research Section B: Beam Interactions with Materials and Atoms, 2003, 202: 182–187
123. Hamaguchi S, Dalvie M, Farouki R T, Sethuraman S. A shock-tracking algorithm for surface evolution under reactive-ion etching. Journal of Applied Physics, 1993, 74(8): 5172–5184
124. Ichikawa T, Yagisawa T, Furukawa S, Taguchi T, Nojima S, Murakami S, Tamaoki N. Cooperative simulation of lithography and topography for three-dimensional high-aspect-ratio etching. Japanese Journal of Applied Physics, 2018, 57(6S2): 06JC01
125. Guo W, Sawin H H. Etching of SiO_2 in C_4F_8/Ar plasmas. I. Numeric kinetics modeling and Monte Carlo simulation in a three-dimensional profile simulator. Journal of Vacuum Science & Technology A, 2010, 28(2): 250–258
126. Marcinkevičius A, Juodkazis S, Watanabe M, Miwa M, Matsuo S, Misawa H, Nishii J. Femtosecond laser-assisted three-dimensional microfabrication in silica. Optics Letters, 2001, 26(5): 277–279
127. Chen F, Deng Z F, Yang Q, Bian H, Du G Q, Si J H, Hou X. Rapid fabrication of a large-area close-packed quasi-periodic microlens array on BK7 glass. Optics Letters, 2014, 39(3): 606–609
128. Bian H, Wei Y, Yang Q, Chen F, Zhang F, Du G Q, Yong J L, Hou X. Direct fabrication of compound-eye microlens array on curved surfaces by a facile femtosecond laser enhanced wet etching process. Applied Physics Letters, 2016, 109(22): 221109
129. Liu X Q, Yu L, Yang S N, Chen Q D, Wang L, Juodkazis S, Sun H B. Optical nanofabrication of concave microlens arrays. Laser & Photonics Reviews, 2019, 13(5): 1800272
130. Liu X Q, Yang S N, Yu L, Chen Q D, Zhang Y L, Sun H B. Rapid engraving of artificial compound eyes from curved sapphire substrate. Advanced Functional Materials, 2019, 29(18): 1900037
131. Zhou T F, Liu X H, Liang Z Q, Liu Y, Xie J Q, Wang X B. Recent advancements in optical microstructure fabrication through glass molding process. Frontiers of Mechanical Engineering, 2017, 12(1): 46–65
132. He Y P, Zhou T F, Kumar A S, Wang X B, Yan J W. Study on the non-free plastic shear removal of material and cutting-induced deformation of micron-submicron grooves. Journal of Materials Processing Technology, 2023, 317: 117999
133. Chen J N, Chen Z Z, Yang Z K, Zhu L M, Zhang Z, Zhang X Q. Fabrication of the curved Fresnel lens array on the spherical surface by 6-axis diamond ruling. Journal of Materials Processing Technology, 2024, 324: 118255
134. Li Q Y, Zhou T F, Zhou J, Hu J J, Zhao B. Ultra-precision cutting of photoresist mask for ultra-smooth surface. Optics and Precision Engineering., 2023, 31(13): 1909–1921
135. Erbas B, Conde-Rubio A, Liu X, Pernollet J, Wang Z Y, Bertsch A, Penedo M, Fantner G, Banerjee M, Kis A, Boero G, Brugger J. Combining thermal scanning probe lithography and dry etching for grayscale nanopattern amplification. Microsystems & Nanoengineering, 2024, 10(1): 28
136. Chou S Y, Krauss P R, Renstrom P J. Imprint of sub-25 nm vias and trenches in polymers. Applied Physics Letters, 1995, 67(21): 3114–3116
137. Guo L J. Recent progress in nanoimprint technology and its applications. Journal of Physics D: Applied Physics, 2004, 37(11): R123
138. Nikolajeff F, Hård S, Curtis B. Diffractive microlenses replicated in fused silica for excimer laser-beam homogenizing. Applied Optics, 1997, 36(32): 8481–8489
139. Suleski T J, Kolste R D T. Fabrication trends for free-space microoptics. Journal of Lightwave Technology, 2005, 23(2): 633–646
140. Jin P, Gao Y L, Liu T T, Li X J, Tan J B. Resist shaping for replication of micro-optical elements with continuous relief in fused silica. Optics Letters, 2010, 35(8): 1169–1171
141. Haynes C L, Van Duyne R P. Nanosphere lithography: A versatile nanofabrication tool for studies of size-dependent nanoparticle optics. The Journal of Physical Chemistry B, 2001, 105(24): 5599–5611
142. Jiang P, McFarland M J. Wafer-scale periodic nanohole arrays templated from two-dimensional nonclose-packed colloidal crystals. Journal of the American Chemical Society, 2005, 127(11): 3710–3711
143. Zhu J, Yu Z F, Burkhard G F, Hsu C M, Connor S T, Xu Y Q, Wang Q, McGehee M, Fan S H, Cui Y. Optical absorption enhancement in amorphous silicon nanowire and nanocone arrays. Nano Letters, 2009, 9(1): 279–282